Catalysis resolved using scanning tunnelling microscopy

Michael Bowker

Received 19th January 2007
First published as an Advance Article on the web 21st May 2007
DOI: 10.1039/b412139m

The technique of scanning tunnelling microscopy has revolutionised our understanding of surface chemistry, due to its ability to image at the atomic and molecular scale, the very realm at which chemistry operates. This *critical review* focuses on its contribution to the resolution of various problems in heterogeneous catalysis, including surface structure, surface intermediates, active sites and spillover. In the article a number of images of surfaces are shown, many at atomic resolution, and the insights which these give into surface reactivity are invaluable. The article should be of interest to catalytic chemists, surface and materials scientists and those involved with nanotechnology/nanoscience. (129 references.)
The graphical abstract shows the reaction between gas phase methanol and oxygen islands on Cu(110), courtesy of Philip Davies of Cardiff University. The added-row island is shown as silver-coloured spheres (copper) and red (oxygen) on the copper surface. Methanol preferentially reacts with the terminal oxygen atoms in the island forming adsorbed methoxy and OH groups. Only the terminal oxygen atoms in the island are active sites for the reaction.

1. Introduction—the development of STM

Microscopy was based on optical methods until the 1930s, and was confined by the Abbé limit for diffraction to a resolution of $\sim$1 μm or so. Such traditional far field microscopies are limited because the propagating waves which are imaged have low spatial frequencies ($<2/\lambda$). In the 1930s electron microscopy was developed by Ernst Ruska[1] to overcome this limit by the use of shorter wavelength electrons of higher energy. The first truly atomically-resolving technique was invented in the 1940s and 50s by Erwin Muller,[2] with the advent of the very different methods of FEM (field emission microscopy) and FIM (field ion microscopy) and one of the first atomic images from the latter is shown in Fig. 1a. This is a beautiful image of the apex of a very fine W needle and this is compared with a more recent image of a Pt tip from Norbert Kruse's group in Brussels. Over the following years electron microscopy improved in spatial resolution and TEM (transmission electron microscopy) is now routinely used for atomic resolution studies of materials, including catalysts (see Fig. 2, for instance[3]).

A major development in microscopy occurred with the invention of the scanning tunnelling microscope (STM) at IBM Zurich in the early 1980s, the first images from the method being published in 1982.[4,5] Binnig and Rohrer were awarded the Nobel Prize for Physics for their invention in 1986,[6,7] and Ernst Ruska was finally recognised too in that prize for his invention of electron microscopy.[7,8] The Nobel lectures give excellent reviews of the invention and early development of STM.[6,7] The technique has evolved since then and Fig. 3 shows a comparison of the first STM image of Si(111), which just about revealed the unit cell on the surface (Fig. 3a[9]), with detailed atomic imaging using improved modern equipment and methodology (Fig. 3b[10]).

SPM (scanning probe microscopy) is now an enormous global business, both industrially (there are now a large number of SPM manufacturers) and academically. It is impossible to present a review of the huge range of application

Wolfson Nanoscience Laboratory, School of Chemistry, Cardiff University, Cardiff, UK CF10 3AT

Michael Bowker

Michael Bowker is Director of the Wolfson Nanoscience Laboratory in the School of Chemistry at Cardiff University and heads the Heterogeneous Catalysis and Surface Science Group. His research covers the fields of nanoscience, surface science and catalysis. He has previously worked in academic (Stanford, Liverpool and Reading Universities) and industrial positions (ICI).

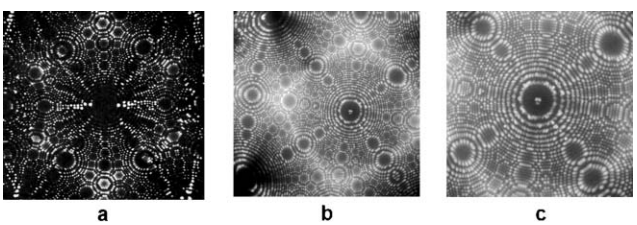

Fig. 1 Examples of FIM images: a) an original Erwin Muller image of a W tip; b) more recent images from Norbert Kruse's group in Brussels showing the detailed atomic structure of a Pt tip, the central area is expanded in c). Images b) and c) are of a (001)-oriented Pt crystal tip, imaged at a field strength F = 37 V nm^{-1} in Ne gas at a specimen temperature of 50 K. Radius of curvature $\sim$65 nm.

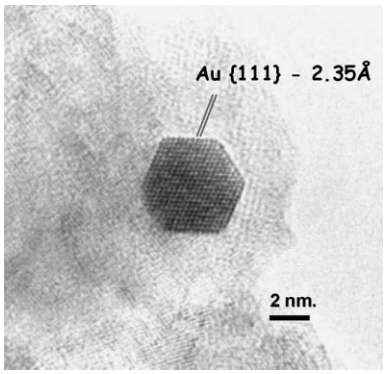

Fig. 2 Transmission electron micrograph, showing atomic resolution of the lattice positions in a Au nanoparticle supported on titania, which makes a very active catalyst for the removal of CO at ambient temperature.[3] © 2005 with permission from Elsevier.

of these techniques in a few pages. The purpose of this contribution is simply to highlight the developments in STM with reference to its application to the understanding of catalysis. STM can be described as a 'nanotool', and catalysis is a nanotechnology, so the application of this method to catalysis is both natural and appropriate, as described more fully below.

2. STM—how it works

Fig. 4 presents a schematic summary of the STM technique, more detailed descriptions can be found elsewhere.[11–13] The method, in common with other SPM (scanning probe microscopy) methods, involves the use of a nanoscale probe (in STM it is usually a metal tip of some kind), combined with a driver facility, which can move the probe with sub-Ångstrom accuracy, all connected to an accurate amplifier system and computer control of the tip movement.

The reason that STM can be so successful for *atomic* resolution is that the tunnelling is an extremely local phenomenon, being essentially confined to the apex atom of the STM tip and to the surface immediately below it. It is an amazing fact that single atoms at the end of a tip are reasonably stable. It may have been imagined, before the advent of the technique, that such a method would be impracticable because of the fluxional nature of the end atom

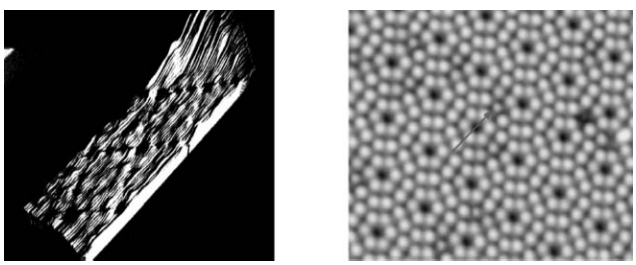

Fig. 3 STM images of the surface of Si(111), contrasting the original image of Binnig and Rohrer (a), which barely shows the (7 × 7) unit cell,[4–6] with a more recent one from Stipe *et al.*[10] (b). The latter shows the detailed structure of the (7 × 7) reconstruction, which had previously been the subject of intense debate. ©American Physical Society 1983 and 1997.

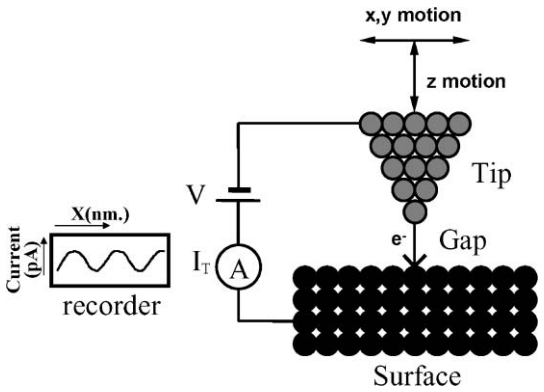

Fig. 4 Schematic diagram of the STM technique. Electrons are shown flowing from the tip to the sample, which would be the case with positive sample bias. As the tip is moved laterally along the surface at constant height, so the measured current oscillates with the atomic position, reflecting the empty electronic states distribution on the atoms. The scan consists of a series of such lines at different positions in the orthogonal direction, to produce a contour 'map' of the surface.

under ambient temperature conditions. However, this appears generally not to be the case, and it is usually obvious when two or more atoms are involved in the tunnelling, because multiple imaging occurs (see Fig. 5 by way of example). The tunnelling current measured has an exponential dependence on distance from the surface, so significant current is only measured at close approach of the tip, say at <0.5 nm from the surface. Another essence of the technique is obviously the ability to scan the surface which, if atomic resolution is to be obtained, must be carried out at sub-Ångstrom resolution. The advent of

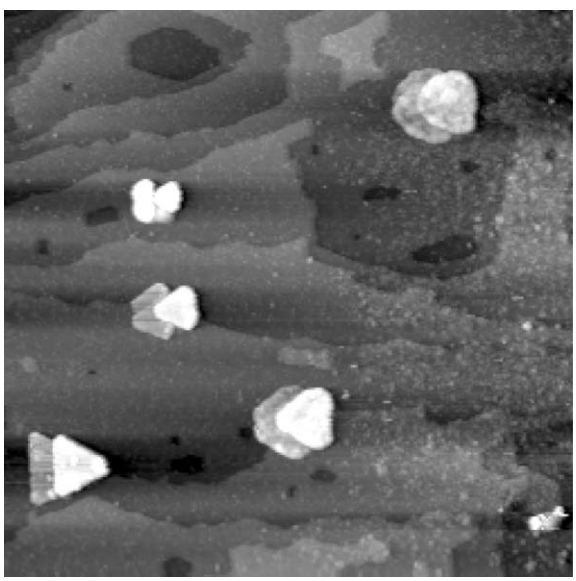

Fig. 5 An example of multiple imaging, for Pd nanoparticles on TiO_2(110); in this case there appear to be three 'tips' giving slightly offset images (particularly evident in the triangular particle in the middle left).[15] Note that good resolution of the underlying oxide structure, especially the steps is obtained, indicating that one of these tips dominates the imaging for a flat surface (that is, it is the closest to the surface).

piezoelectric scanners has enabled this to be the case. Piezoelectric scanners are usually of two types—the tripod scanners, basically consisting of three (x, y, and z tip movement) linear scanners, or tube scanners, which depend on the bending of a piezo-cylinder when radial potential differences are applied for x and y movement, while control of the z movement (tip approach to the surface) involves an axial potential difference. The typical response of such piezos is $\sim$1 Å per V applied.[12] When the tip has approached sufficiently closely to the surface (less than $\sim$10 Å) by increasing the voltage to the Z drive, then a tunnelling current (usually $\sim$ a few pA) can be detected and amplified.

Scanning usually involves a feedback system so that the tip z-position responds to the tunnelling current (constant current mode). If the tunnelling current increases as the tip is moved parallel to the surface, then the feedback pulls the tip back to reduce it again to a constant value, and the z voltage applied to enable this is then the measure of surface topography. It is very important to note that what is meant by topography in STM is actually the density of electronic states at the surface under the tunnelling conditions used. In the case of positive sample bias, tunnelling then usually occurs into empty states in the sample whereas reverse bias results in tunnelling from filled sample states into empty states on the surface of the tip (see Fig. 6). In this respect it's also worth noting that, although it is common for the peaks in electron density to be associated with atomic topography on the surface, there are notable exceptions and it is possible to go very wrong with simple interpretations of peaks of tunnelling or Z position as being associated with atomic positions on the surface. By way of example Stroscio *et al.* showed early on that the apparent atomic positions for the (2 × 1)-reconstructed Si(111) surface were displaced by exactly ½ a lattice spacing from the real location of the surface atoms under certain bias conditions (Fig. 7[14]). However, it is more often the case that real atomic positions are revealed, though the nature of the image, particularly the contrast, can be very variable, even within a single image (see Fig. 8 for example[15]), mainly due to changes in the chemical nature of the tip, by pick-up or loss of atoms from it.

The tunnelling current can be approximated by the following simple equation,[11–13,16] at least for tunnelling between s-states at the surfaces:

$$I = \mathrm{f}(V).\ \exp^{(-2(\sqrt{2m\varphi})z/\hbar)}$$

Where I is the tunnelling current, f(V) is a bias-voltage dependent pre-exponential factor, m is the electronic mass, φ is the effective local work function and z is the tip-surface separation; and hence the stark dependence of tunnelling current on the tunnelling gap, dominated by the exponential term.

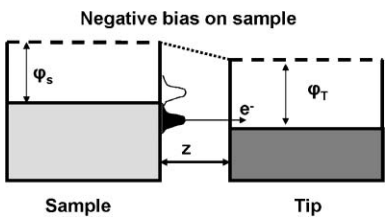

Fig. 6 Band diagram of tunnelling, in this case showing the situation for negative sample bias, resulting in tunnelling from the sample to the tip; φ is the work function, and z is the tip-surface spacing.

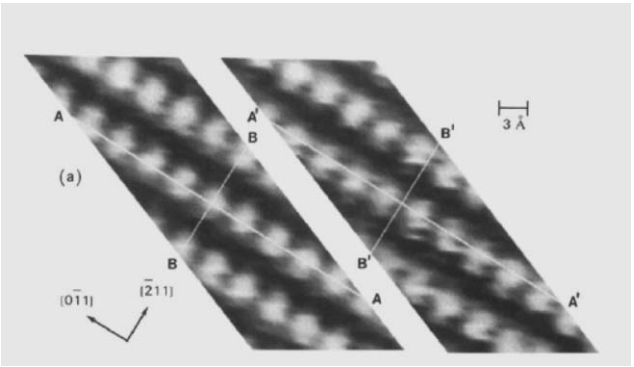

Fig. 7 Constant current STM images of the Si(111) – (2 × 1) reconstructed surface, obtained at bias voltages of +0.7 V (right) and −0.7 V (left), showing the dominance of electronic structure in the images, which can give a false impression of atomic positions.[14] The maxima in intensity are shifted by ½ of a lattice position between the two images in the (−2,1,1) direction (lines A ans A′), and so it is apparent that both cannot represent the true atomic positions. ©American Physical Society 1986.

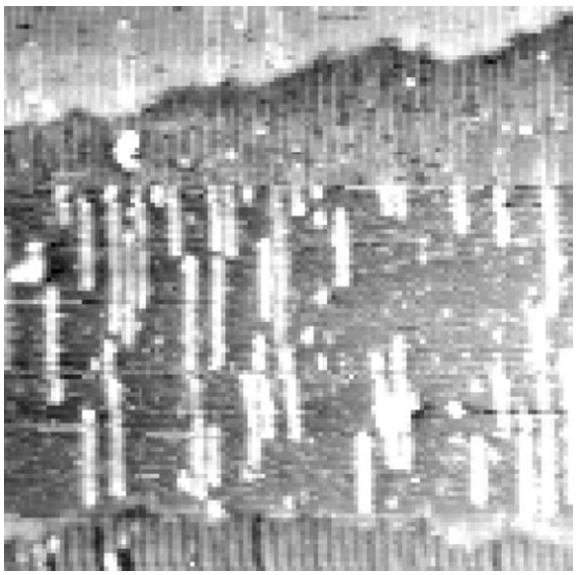

Fig. 8 An image of the TiO_2(110) surface, showing varying contrast and apparent surface structure, due to sudden changes in tip composition/morphology.[15] The surface is mainly the (1 × 2) structure, but with added strings of titania on the surface.

Although chemical information is not easy to obtain by STM, contrast between different atoms can often be seen (in alloys, for instance, as described in section 6i below), due to the different local electronic structure around dissimilar elements. However, detailed information can be obtained by determining the dependence of current upon applied tip voltage, preferably obtained at constant tip height. A variety of such approaches can be applied, going by the general name of scanning tunnelling spectroscopy, and STS is described in more detail elsewhere.[11–13] In general terms, Ohmic behaviour is usually found for good conductors, and semiconductors depart from

the linear shape of the *I–V* curves, reflective of the band gap. Further, details within these curves can reveal inelastic energy loss processes, even down to the ability to resolve vibrational transitions,[17] which can provide some chemical information for molecular adsorbates, at least in favourable cases and conditions.

3. Problems with the application of STM and (to some degree) overcoming them

This article concentrates on the successes of STM and surface science applied to catalysis. However, it is important to note some major drawbacks of the technique. The most important points of limitation are i) sample conductivity and ii) sample roughness. The first is an essential drawback of STM; the sample must have reasonably good conductivity for tunnelling to occur. Thus insulating samples cannot be studied, and many types of catalysts consist of active phases supported on insulating supports such as alumina and silica. This problem is overcome, to a degree, by the use of very thin, model supports fabricated onto a conducting substrate, and this is considered in more detail in section 6ii below. Regarding sample roughness, it must be remembered that a surface with troughs and valleys of the order of a micron in size appears, to an STM tip, like a mountain range. It is very difficult for the tip, feedback and imaging system to cope with surface asperities and they are generally damaging to the tip itself due to collisions (it must be noted that, on the nano-scale, the tip has high velocity across the surface, typically $\sim 10^{-6}$ m s^{-1}, which sounds very slow in macroscopic terms, but which is actually $\sim$3000 atoms imaged per second). Further, care has to be taken in the interpretation of rough features on a surface, including nanoparticles, since convolution of topography between the tip itself and the nanoparticle occurs, resulting in over-estimation of the nanoparticle size.[18,19] This convolution happens because the periphery of the tip region remote from the apex tip atom, which is that involved in the tunnelling, interacts with the particle first, and so the tip begins to raise from the surface plane before the apex atom has reached the edge of the particle. Real catalysts are usually very rough materials, in powdered form, and so it is generally impossible to image real catalysts, though it has been attempted in some particular cases (as described in section 7.5 below).

4. The major advantages of STM

1. Atomic resolution

The major advantage of STM, and the reason for its wide-scale application, is the ability to image atoms, molecules and nanoscale features at surfaces. This is particularly important in relation to catalysis and chemistry, as described in more detail in section 5 below.

2. Local Information and high sensitivity

STM is not a surface averaging technique, in contrast to most of the other techniques used in surface science. For example, for a surface which is perfect, but which has $\sim$1% defect sites, the defects will usually not be detected by XPS, whereas each site can be identified in an STM image. In this sense STM is a very precise technique and in principle every atom in an imaged area can be identified. For example, see Fig. 3.

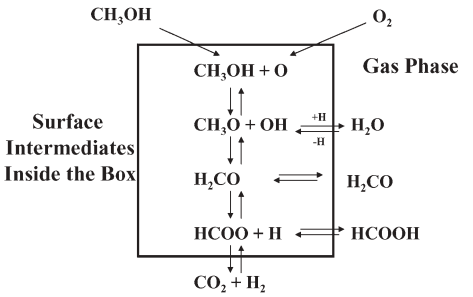

Fig. 9 Schematic diagram of the various reaction steps in the selective oxidation of methanol.[21]

3. Wide range of environments

A further advantage is the ability to image in a wide range of environments, including liquids, and it has the possibility for *in-situ*, and even *in-operando* imaging. A major objective of STM in relation to catalysis is the latter, to see the structure of surfaces, if possible, as a reaction takes place. STM has even been carried out in aggressive electrochemical environments,[20] though tips do not usually last very long in that situation. Examples of catalytically-related work at high temperature and pressure are given in section 8 below.

5. Catalysis and chemistry – molecular sciences.

Chemistry is a molecular science. More specifically, right from our school days we are used to presenting chemical reactions in a molecularly descriptive fashion. Consider, for instance the catalytic selective oxidative dehydrogenation of methanol, which we write stoichiometrically as:

$$CH_3OH + 1/2O_2 \rightarrow H_2CO + H_2O$$

Although we can write the reaction in terms of molecules, nobody has 'seen' a molecule of methanol react with oxygen in this way. Reaction equations are derived from the results of global reaction measurements and considerations of stoichiometry. The details of the way in which these molecules react can not be seen, but the advent of STM, for the first time, allows us the possibility of direct insight into the reaction at the atomic scale, albeit on solid surfaces. By way of example, Fig. 9 shows a sequence of reaction steps for the reaction of gas phase methanol with oxygen on a copper surface.[21] This produces methoxy groups as the first step, in which the slightly acidic hydrogen from the alcohol is stripped by surface oxygen in the following steps, where the subscript a refers to adsorbed species

$$CH_3OH + O_a \rightarrow CH_3O_a + OH_a$$

$$CH_3OH + O_a \rightarrow CH_3O_a + H_2O$$

The removal of oxygen atoms from the surface of Cu(110) occurs in a very particular way, revealed by the STM, as

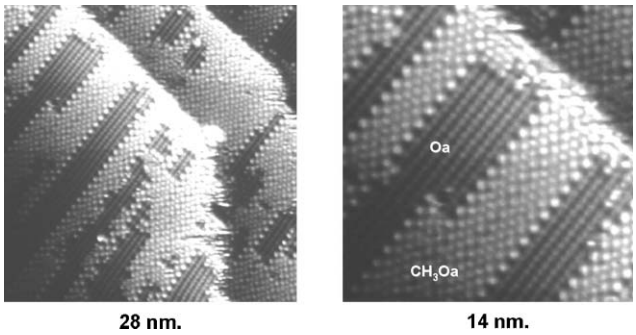

Fig. 10 STM image of a Cu(110) surface with both oxygen islands and methoxy groups present after dosing oxygen on the surface, followed by methanol. A methoxy area is labelled as CH_3Oa and an atomic oxygen island as Oa. Note that the two species are phase-separated on the surface.[21–24] © 1994with permission from Elsevier.

described in more detail in section 7.1 below. Fig. 10 shows a reaction part way to completion, in which both oxygen structures and methoxy structures can be identified and are seen to co-exist on the surface.[22–25] The oxygen is eventually completely removed by methanol exposure and is replaced by methoxy groups, also described in more detail in section 7.1 below. This kind of reactivity of Cu has been confirmed by others.[26]

6. Model catalysts and their fabrication

As described above a disadvantage of the STM technique is the need for flat, conducting surfaces for good imaging, which is in contrast to the nature of industrial catalytic materials, which tend to be very heterogeneous powders, rough and more often than not, insulating as described above. Ingenious ways of studying catalysts have been developed which get round these problems to a degree, namely the use of model conducting catalytic materials.

These model catalysts can be of several types:

i) Single crystals

ii) 'Inverse' catalysts

iii) Nanoparticulate model catalyst surfaces

iv) Ordered nanoparticulate surfaces

and they are described in this order in what follows.

i) Single crystals

Single crystals have been the mainstay of surface science studies from the beginnings of the modern era of the subject, dating from the mid 60s when such crystals became more widely available. They are extremely useful for study because they present the investigator with a very well-defined interface in which the atomic positions of the surface atoms can usually be predicted, and therefore one aspect of the experiment can be pinned down immediately. The basic work on the structure and reactivity of many single crystal surfaces was carried out in the latter part of the 20th century. However, low index crystals of the type shown in Fig. 11 are not very closely related to the heterogeneous materials which often present 'real' surfaces in everyday life, and particularly in catalysis, since the coordination number of the atoms on a (111) plane, for instance, is

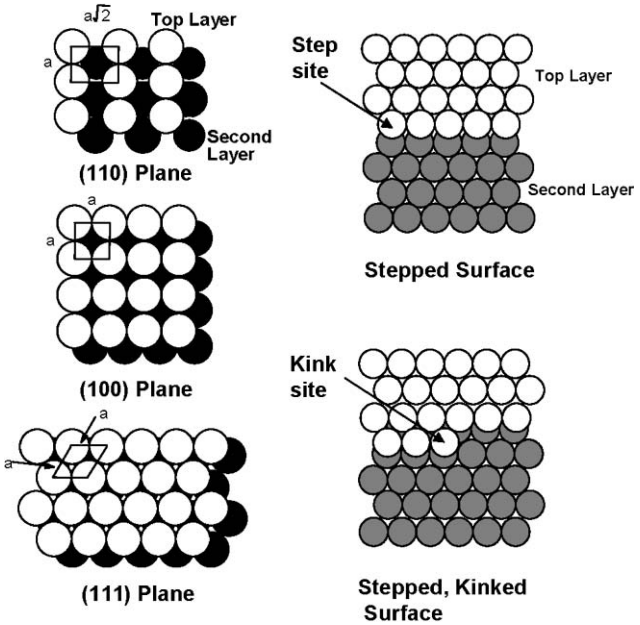

Fig. 11 Models of fcc crystal surfaces. Left, low index, simple surfaces; right, stepped and kinked surfaces, based on the (111) close-packed plane.

nine, whereas that for a small catalytically active nanoparticle is much lower. Advances were made in the study of surface reactions by using high Miller index single crystal planes (see Fig. 11), pioneered by Somorjai[27–29] and others,[30–32] so that some idea of the influence of varying surface coordination on surface reactivity could be assessed. Single crystals of a wider variety were developed, including alloys and some oxides, which further extended the range of surface science investigation. Although it is often said that STM is not chemically specific, it is possible to identify different types of atoms due to their different contrast in STM images, and their different electronic response, as described theoretically early on by Lang[33] and experimentally by Ruan *et al.*,[34] for instance, for oxygen adsorbed on Ni and Cu crystal surfaces. Examples of beautiful images of alloy surfaces, in which two metal atoms comprising the alloy can be distinguished, are shown in Fig. 12.[35–37] Obviously, due to the very local effect of tunnelling, the local electronic structure on individual atoms

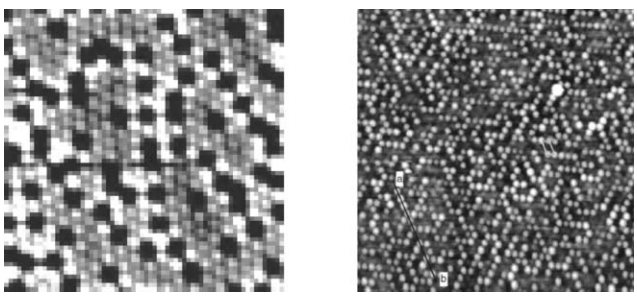

Fig. 12 Examples of atom discrimination in STM for alloy surface structures. Left, a Au/Ni hexagonal surface with the Ni imaged as the bright atoms,[35] ©American Physical Society 2005, and right a Co/Pt surface with Pt atoms imaged as the bright features,[36] © 2000 with permission from Elsevier.

can be distinguished. However, such materials are neither supported, nor are they nanoscale objects, and so, in order to study materials more closely related to heterogeneous catalysts, some further developments were required.

ii) 'Inverse' catalysts

These developments include the 'inverse catalyst' concept and nanoparticulate surfaces (the latter are described in section iii below). The 'inverse catalyst' idea involves the formation of oxide films, usually produced on the surface of metal single crystals [for reviews, see ref. 38–40]. They are 'inverse' because, effectively, they are composed of oxides supported by metals, which is the opposite of the usual situation for commercial catalysts, which are metals supported on oxides. Early examples of such materials include ThO_2 supported on Au,[41] TiOx supported on Rh[42] and ZnO supported on Cu.[43,44] Because the oxide film is very thin, materials which would otherwise be insulating can be studied by STM, since tunnelling can still occur, with charging limited by electron exchange with the underlying metal. The thickness of the film through which tunnelling can be imaged depends very much on the electronic structure of the insulator. Thus, for example, layers of a wide band-gap insulator such as CaF_2 have been imaged on Si at a thickness of as much as 3 nm, because, although the band-gap is $\sim$12 eV, nonetheless, since the conduction band of CaF_2 is $\sim$3 eV above the Fermi level, it is accessible to STM.[45]

Examples of inverse catalysts include those made by Boffa *et al.* who produced thin titania layers on Pt(111),[46] while Netzer *et al.* have fabricated vanadium oxides of various stoichiometry on Pd single crystal surfaces (Fig. 13[47]), Bowker *et al.* have produced BaO layers on Pt(111) (Fig. 13b,[48]), and a number of others have worked on alumina thin films (Fig. 14).[38,50,52–56] The BaO structure is particularly interesting because the surface manifests the BaO(111) – (2 $\times$ 2) surface

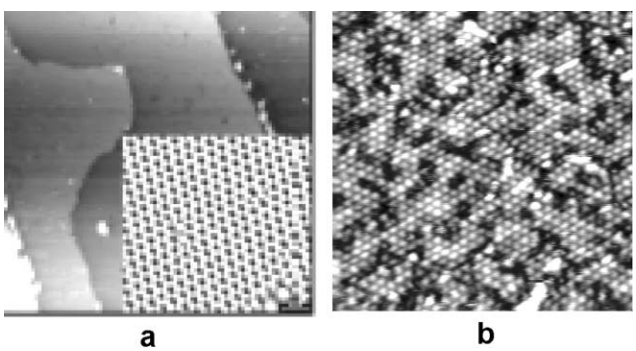

Fig. 13 (a) STM image of a model vanadium oxide surface consisting of 0.2 monolayer of V-oxide on a Pd(111) surface.[47] The V-oxide/Pd(111) surface was annealed to 250 °C in UHV after the oxide deposition and covered to 40% by s-V_2O_3 phase islands ((100 $\times$ 100 nm); the inset is an 8 $\times$ 8 nm high-resolution STM image of the s-V_2O_3 phase). With kind permission of Springer Science and Business Media. (b) Image of a model BaO surface, consisting of a hexagonal layer of BaO(111) showing a (2 $\times$ 2) reconstruction,[48,49] 25 $\times$ 25 nm. The spacing between the bright spots in the image (0.81 $\pm$ 0.02 nm) is about twice that expected for the (1 $\times$ 1) termination (0.39 nm.); © 2006 with permission from Elsevier.

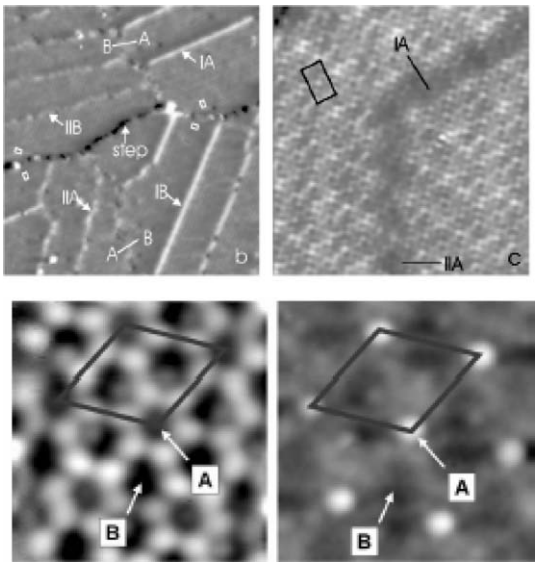

Fig. 14 Alumina thin film STM. The top two images show the work of Freund *et al.*[52,53] making thin films on the NiAl(110) surface, which forms domain boundaries between domains (the bright bands), with a step running across the middle of the top left hand image, ©American Physical Society 2003. The lower images are from the work of Degen *et al.*[55,56] on NiAl(111), showing the structure as a network, with large variations in imaged structure with tip bias; © 2006 with permission from Elsevier.

reconstruction expected on theoretical grounds due to its low surface energy and the instability of the polar (1 $\times$ 1) termination.[51]

Freund and co-workers have developed a number of such materials to use as ordered model supports, most notable being the extremely thin alumina films prepared by the careful oxidation of NiAl(110) single crystals,[50,52,53] Fig. 14. There has been much discussion of the detailed structure of these alumina films, since most catalysts supported on alumina use the high surface area γ-alumina phase. Recently it has become apparent that this alumina film is special and probably oxygen-deficient[54] and maybe closer in structure to ε-alumina. As shown in Fig. 10, the film has ordered arrays of defects on the surface, and these are due to phase domain boundaries between crystallites of alumina on the surface. This occurs due to strain in the adlayer. Note that such thin alumina films can also be prepared on NiAl(111); this produces more perfect surfaces as shown by Becker and Wandelt (Fig. 14) who produced alumina films $\sim$0.5 nm thick.[55,56] Goodman has managed to prepare well-ordered thin films of silica onto a Mo(112) single crystal surface, Fig. 15.[57,58] One of the useful properties of such films is that they can be removed again by Ar ion sputtering to yield the clean metal substrate which can be oxidised to produce a new film. In many cases oxide surfaces can be prepared on refractory metal substrates, so that they can be removed simply by heating to high temperature.

In a remarkable development which is along these lines, Besenbacher and his colleagues at Aarhus in Denmark have fabricated model catalysts of monolayer MoS_2,[59–61] and have made such samples with Co incorporated too. They have been

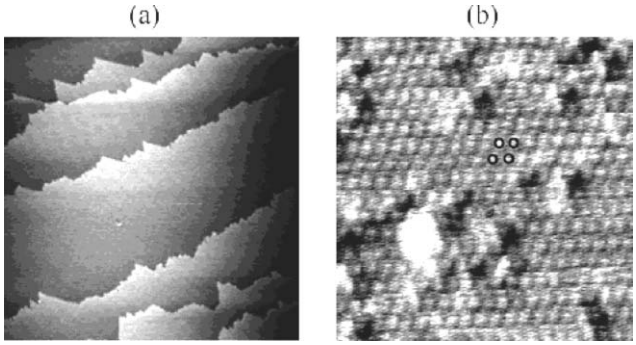

Fig. 15 STM images of a thin silica film annealed to 1200 K, showing the c(2 × 2) array of the surface lattice (indicated by the circled points on the right hand image); and steps on the surface in the left hand image, from the work of the Goodman group at Texas A&M.[54] The ordered, ultrathin SiO_2 films with a thickness of 0.35 nm were synthesized by vapour deposition of Si onto an oxidised surface of Mo(112), with further post-oxidation at 800 K, and an anneal in oxygen at 1100–1200 K.

produced on a Au(111) surface in order to investigate some of the details of a very important industrial catalytic process. This is hydrodesulfurisation, carried out on the very grand scale indeed in refineries across the globe to reduce the harmful sulfur levels in oil-based feeds used for the production of a range of useful hydrocarbons, including fuel for vehicles. This is important both for the protection of other catalysts further in the refining processes (such as the Pt reforming catalysts) and for environmental protection by producing low sulfur fuel. There has been much discussion about the nature of the active site for this reaction, but such materials had not been observed in a reacting environment before. As shown in Fig. 16 Besenbacher *et al.* were able to make such nanocrystalline materials, but not only that, they could observe the catalyst structure at atomic resolution, and even look at active sites in the reaction (see section 7.1 below). The crystallites of MoS_2 are triangular, and manifest a near-hexagonal surface symmetry. They are proposed to be composed of a single layer of MoS_2, comprising a three layer sub-assembly of Mo sandwiched between two sulfur layers, with the lower layer of S directly interacting with Au crystal. In Fig. 16, it is considered that the surface S atoms are imaged and that a triangular band around the outside of the particle is due to an enhanced electron density at the edge of the particle. The Aarhus group was also able to make the mixed Co–Mo sulfide and such a particle is shown in Fig. 16, with the Co atoms segregated to particular edge positions in the structure, changing the particle morphology.

iii) Nanoparticulate surfaces

The developments above are very welcome, but most heterogeneous catalysts consist of nanoparticles of an active phase (often a metal) on a relatively inactive oxidic phase. Thus, in more recent times, a number of workers have advanced to study nanoparticulate materials, often fabricated in the same instrument in which they are studied.[62–64] The development of 'inverse catalysts' described above is a precursor to much of this activity because the model catalysts are often prepared in

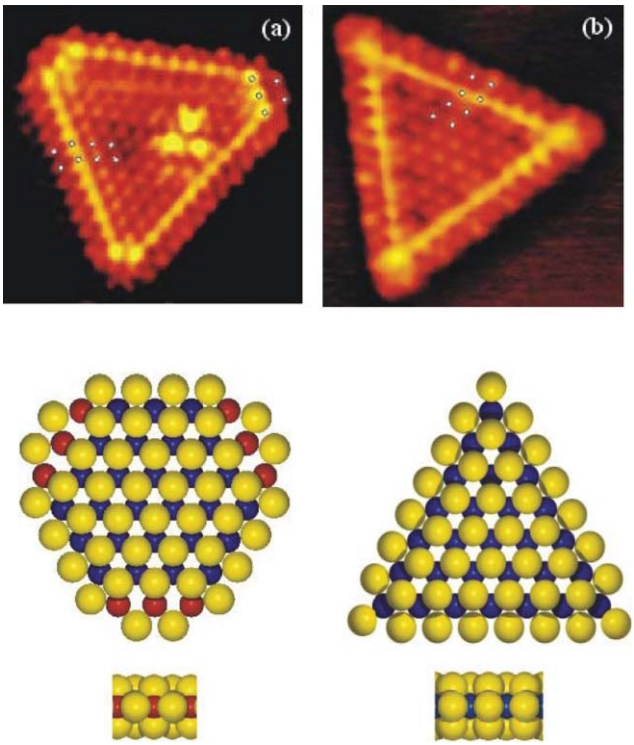

Fig. 16 An image of a thin layer MoS_2 particle fabricated onto a Au(111) surface (right image, b), and a similar particle with Co incorporated (left image, a). The particles manifest the basal plane of MoS_2, and are shown as ball models in the lower part of the figure, in plan immediately below the images, and in elevation in the lower models. Yellow spheres are S atoms, blue are Mo and red are Co. From the work of the Aarhus group.[59–61] © 2001 with permission from Elsevier

three layers, that is, an oxide deposited on a metal substrate, followed by the deposition of metal to form an array of nanoparticles supported on a thin film oxide.[63–66] In Fig. 17

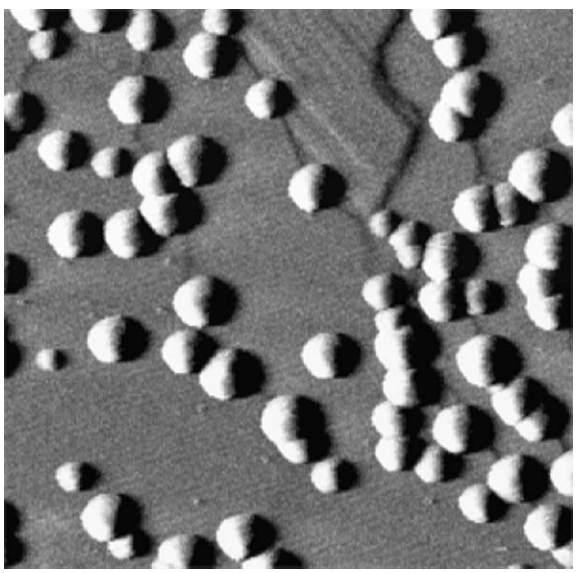

Fig. 17 Three layer catalysts—silver nanoparticles deposited onto the thin alumina film on NiAl(110).[64] Image size 130 × 130 nm. ©American Physical Society 2000.

examples are shown for arrays of silver on thin film alumina formed on Ni–Al(110). These materials can then be used for further study, and especially to interrogate the nature of the centres involved in reaction with gas phase species, as exemplified below.

It is also possible, in some cases, to fabricate model nanoparticulate catalysts on single crystal oxides, and there is now also a significant body of work in this area. A limitation of this kind of work is that for these cases the oxide has to be at least semi-conducting in order to give sufficient tunnelling current. Fig. 18 shows an example of this kind of material—an array of Pd nanoparticles formed onto a TiO_2(110) surface.[67–70] Here the nanoparticles have been formed by deposition of Pd from a heated metal source onto the titania surface at ambient temperature, which is then annealed to 773K, and imaged at 673K. In principle, titania is a wide band gap semiconductor, with little conductivity in its fully oxidised state. However, after sputter and anneal cycles in UHV the sample is sufficiently conducting to enable successful STM imaging. It can be seen that there is some preference for particles formed on such a surface to be located at step edges on the titania, but they are also present on the terraces. It is commonly observed that nanoparticles fabricated in this way do preferentially form on the steps, which act as nucleation sites for forming the critical nucleii. A review of some of the work on nanoparticles supported on single crystal titania is given in an excellent review article by Diebold, which mainly covers the properties, and STM imaging, of titania itself.[71]

iv) Ordered nanoparticulate surfaces

Of great interest in relation to catalysis is the possibility of producing better-defined materials. Commercial catalysts are heterogeneous in many respects. In particular they usually consist of a heterogeneous array of active particles on a (relatively) inert support. These are of varying particle sizes, varying inter-particle distances, varying surface morphology, and often with some variability of the site on the support to which they are anchored. It has been shown in many cases that the efficiency of reaction of a catalyst depends on the particle size, and that the nature of the metal–support interaction and particle spacing can be very important for dictating this efficiency. A notable recent example of this is the extreme size dependence of the turnover of Au nanoparticles for the low temperature oxidation of CO,[72–75] a reaction of great interest for environmental protection and CO removal systems, and considered in more detail in section 7.1 below. Since this is the case it would be advantageous to make catalysts with mono-sized arrays of evenly-spaced particles, perhaps even with a particular geometric relationship to each other.

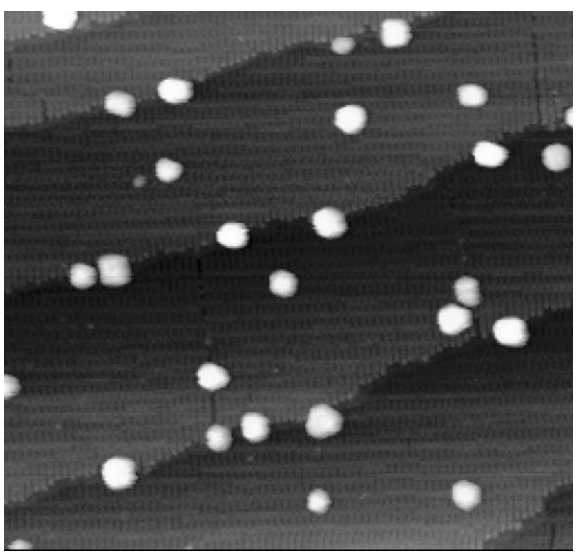

Fig. 18 An STM image of nanoparticles of Pd on TiO_2(110). The particles are ~4 nm diameter.

Attempts are being made to produce model catalysts of this type. Kasemo has produced arrays of Pt particles on ceria surfaces,[76,77] a system of interest in relation to the removal of pollutants from cars. Fig. 19 shows an example of such a material which is produced by electron beam lithography, and shows that quite complex nanoparticle architecture can be incorporated by these methods. The methodology is derived from semiconductor device fabrication, as illustrated by Somorjai,[78–80] Fig. 20, which presents an example of the fabrication of an array of approximately 20 nm diameter particles of Pt, arranged in a square array with a particle separation of 100 nm, imaged by AFM and by SEM. The fabrication of such a layer is a many step process, and so is extremely slow. In this case it involves the deposition of a film of aluminium onto a silicon substrate, followed by oxidation of the film to make the oxidic support. This is then followed by the spin casting of a polymer resist (poly-methyl methacrylate), which decomposes when exposed to an electron beam. The beam is directed to produce a series of dots in the film, which, when washed in solvent are removed, while the cross-linked unexposed polymer areas are not removed. This leaves the polymer film with a series of holes in it, exposing the underlying alumina. If this is then exposed to Pt, and the surface is washed with a solvent which dissolves the polymer, then the series of dots of Pt is left in the original holes in the resist layer. In these cases it is not possible to image the array by STM, since the supports used are insulating, being a 10 nm thick alumina layer.

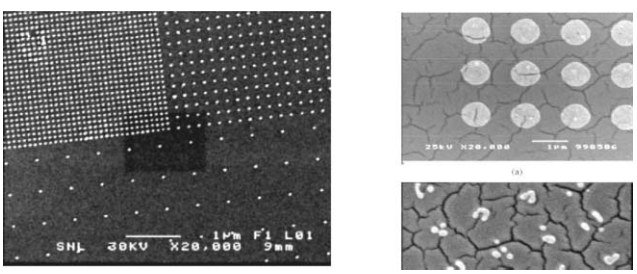

Fig. 19 (Left image), arrays of Pt nanoparticles formed by electron beam lithography, arranged in a square array, with three different spacings, and imaged by SEM;[76,77] reproduced with permission of the Royal Society of Chemistry. On the right the Pt particles are supported on a ceria thin film before (upper) and after (lower) annealing. The bar on the images represents 1 micron in length. With kind permission of Springer Science and Business Media.

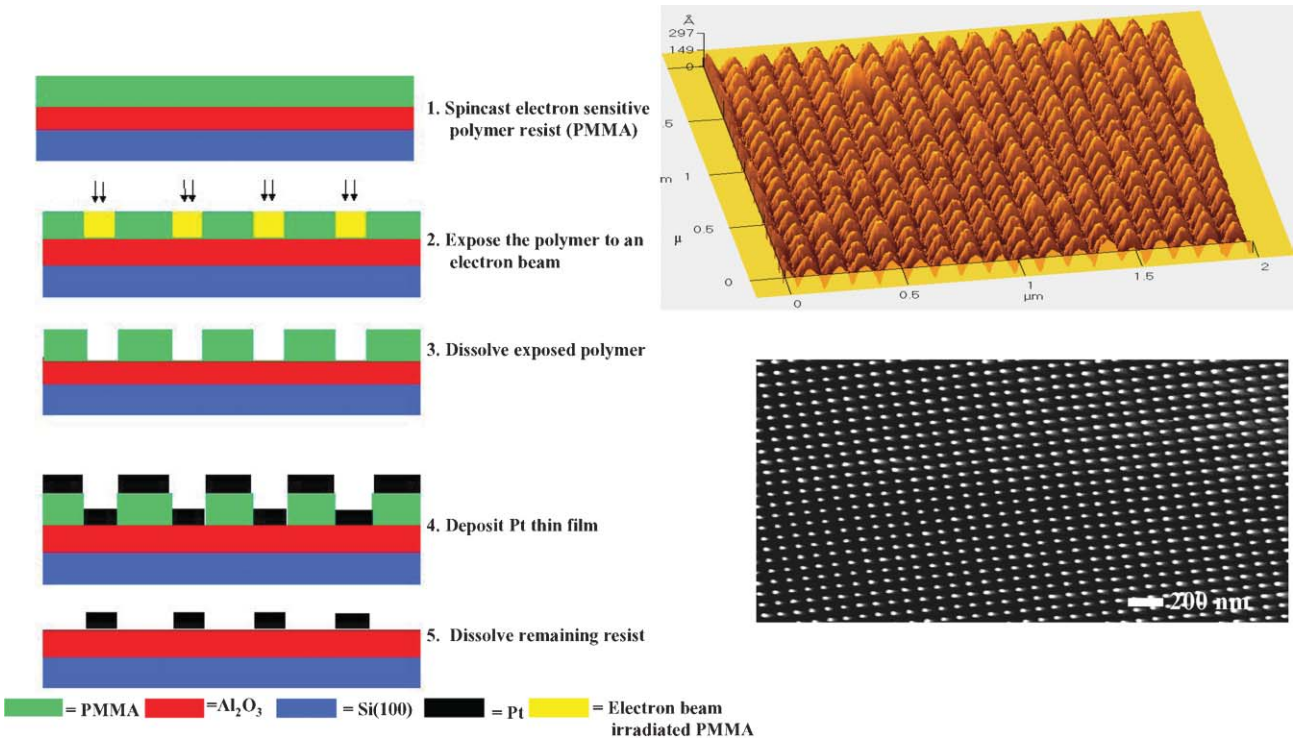

Fig. 20 An array of Pt nanoparticles with a diameter of 28(±2) nm and a periodicity of 100 (±2) nm, fabricated in the way shown in the left hand panel onto an alumina film on a Si single crystal. The particles are imaged by AFM (top right) and SEM (bottom right),[78–80] courtesy of Professor Gabor Somorjai at Berkeley.

Although these materials can be produced there are several problems with them. First of all, electron beam lithography is limited in its resolution. Ideally we would like to make small particles of this type down to ~2 nm diameter, whereas the limit of size produced so far is ~20 nm Secondly, we would like such materials to be thermally stable and resistant to sintering, so that integrity of uniformity is maintained. Kasemo has shown that disruption of the particles occurs in the case of the ceria support when the material is heated (Fig. 19) and thermal stability and the maintenance of integrity of such nanoparticles is a matter of considerable importance and impending developments.

Regarding STM imaging of such materials, that can only be achieved for ordered arrays deposited on conducting substrates, which could include the thin layer oxides described in section 6ii above, and the general problems of imaging nanoparticles described above needs to be addressed by either fast feedback response loops or very slow scanning.

To a degree these factors have been addressed by Becker and Wandelt[55,56,81] who have used the NiAl(111) substrate to make well-ordered, thin layers of alumina. These appear to act as excellent templates for the fabrication of ordered arrays of nanoparticles, which locate themselves preferentially into the ordered depressions on the alumina surface (Fig. 21). For Pd nanoparticles on this surface, they were stable up to temperatures of ~600 K, thereafter they nucleate into islands and lose their individual identity.[56]

In the following sections we will describe the results of catalytically-relevant work which utilises all of these kinds of model catalysts.

7. STM applied to catalytic problems using model catalysts

In what follows we will not consider the wide range of studies of adsorption related to catalysis which has been carried out under standard surface science conditions (usually very low

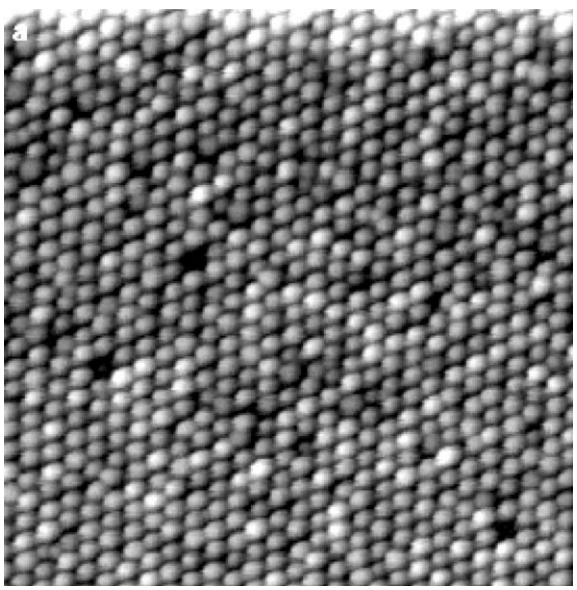

Fig. 21 STM image of an array of Pd nanoparticles deposited onto an alumina film on NiAl(111) (as in Fig. 14) at room temperature;[56] image size 108 × 108 nm. Reproduced with permission of the Royal Society of Chemistry.

pressures and ambient temperature), or at very low temperature. This is the vast majority of the work in this field. Instead, we will focus on work relating to reactions occurring in real-time, or under conditions approaching those in which heterogeneous catalysis takes place (high temperature and pressure), or which use model catalysts more closely related to the nanoparticulate materials used in a reactor. One notable early piece of work was one of the first attempts to study catalysis at high pressure using STM; it was carried out by the Shell group of Wilson and de Groot working in industry, and this showed the potential for such work in catalysis.[82] They investigated the atomic-scale restructuring of Co(0001) single crystal under conditions of 4 bar of a 2 : 1 H_2/CO mix at 523K and found that the well-ordered crystal surface became much less perfect after reaction. Indeed, small particles of Co were present all over the terrace, assumed to be formed by migration of Co sub-carbonyl species. However, these images were obtained at ambient temperature and at low pressure in a post-reaction analysis. In this article we will focus on attempts to study reactions relevant to catalysis *in-situ*, while reacting and under conditions approaching those normally used in catalysis and/or using model nanoparticulate materials.

7.1. STM *in-situ*: attempting to image the 'active site'on single crystals

A great deal of work in relation to this subject has been carried out on Cu crystal surfaces, and especially on Cu(110), partly due to the interesting and unusual surface structure induced by oxygen adsorption at the surface. Oxygen adsorbs to form thin strings of Cu–O atoms which have been seen to be mobile at ambient temperature.[21,83–85] However, as the oxygen coverage increases, so attractive lateral interaction between these strings begin to crystallise the oxygen into islands consisting of groups of these strings (Fig. 22[21,23–25]). The structure of these islands is shown schematically in the first panel of Fig. 24, the important point here being that these islands present several different types of active sites at the surface. There are oxygen atoms in the centre of the island, which are the majority, there are some at the long edges of the island (approximately 30% of the islands shown on Fig. 22) and the minority at the short ends of the islands (about 4%). Nevertheless it is often the atoms at the short end which are the active species. This is shown by the images of Fig. 23, for the reaction of adsorbed oxygen on Cu(110) with gas phase methanol, where the islands shrink from the short ends only.[21–25] The reason this site is more active may be related to the local coordination of the oxygen atom. The oxygen atom at the end of the chain is only coordinated to one surface layer copper atom, whereas the others are all coordinated to two. This limited bonding makes these atoms the active ones. Although the islands shown in Fig. 22 and 23 have only a small percentage of the oxygen atoms as active sites, nonetheless, as one active oxygen atom is removed, so an oxygen atom that was previously not an active site, becomes one by the mechanism shown in Fig. 24. For this to be the case when an oxygen atom is removed from the end of the island a copper atom must be lost from that site to reveal another active oxygen atom at the end. Evidence that this does indeed occur has been shown by seeing a build up of

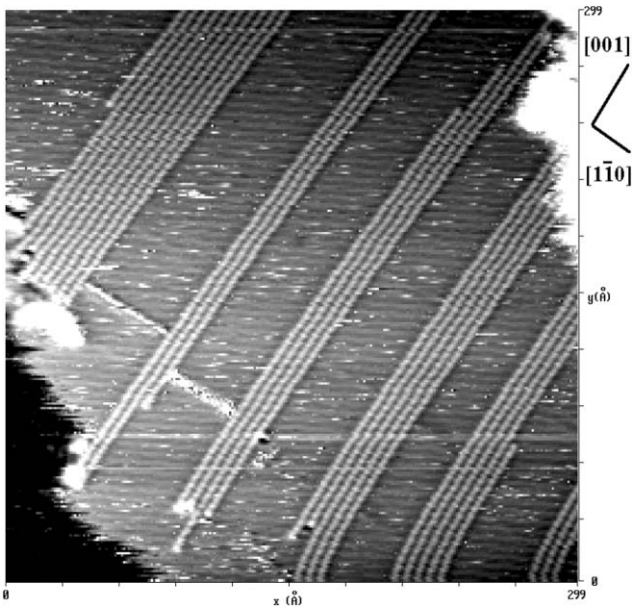

Fig. 22 Oxygen islands on Cu(110). The islands grow with a long aspect ratio, consisting of Cu–O strings oriented in the [001] direction of the surface, with clustering of the strings in the [011] direction, with different numbers of strings in each island.[23–25] Image size, 80 × 80 nm. © 1997 with permission from Elsevier.

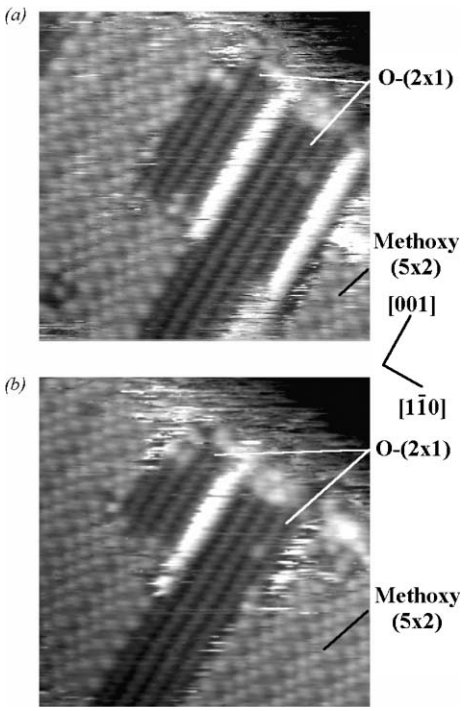

Fig. 23 Two images of the reaction of islands of oxygen on Cu(110) with gas phase methanol. From a to b the island reacts in a particular way, shrinking in the [001] direction as oxygen is removed by reaction with methanol to produce two methoxy groups and gas phase water;[21,23–25] the detailed mechanism is shown in Fig. 24. The white lines are restricted regions of clean Cu on which methoxy is diffusing before forming the ordered methoxy structure. © 1997 with permission from Elsevier.

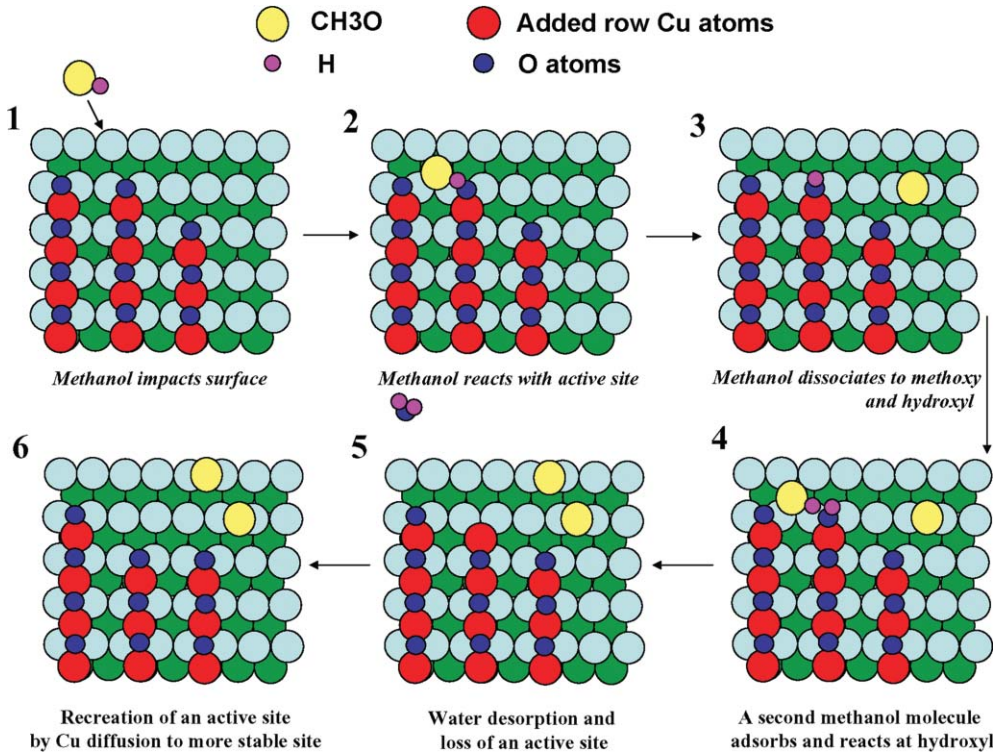

Fig. 24 A reaction model for the initial stages of methanol oxidation on Cu(110). The Cu surface is shown with an added island of oxygen in the (1 × 2) reconstruction with added Cu atoms as red balls and added oxygen as blue. The underlying Cu atoms are shown as light blue and those one layer further below as green; the [001] direction is the vertical on the page, [1,−1,0] is the horizontal. In panel 1—methanol adsorbs on the surface, the methanol is shown as a methoxy group (yellow ball) and a hydrogen atom (magenta); 2,3—an acid–base reaction results in stripping of the terminal hydrogen of methanol to produce methoxy and hydroxy groups; 4,5—another methanol reacts with the hydroxy group to from another surface methoxy and to liberate water into the gas phase, leaving a terminal Cu atom at th end of a chain; 6—the exposed Cu atom diffused away from the terminal site, forming a new active terminal oxygen.

Cu at steps near to the reactive islands during the reaction.[22] Similar reactivity has been shown by Davies *et al.* who are engaged in a comprehensive survey of organic molecule reactivity with such surfaces.[86–88] Fig. 25 shows STM images during the reaction of trifluoroethylamine with oxygen islands on Cu(110) in which the oxygen is removed by reaction with the organic in a similar way to methanol, with preferential reaction at the end atoms of the chain, thus showing one-dimensional shrinkage of the islands.[21]

In a similar vein, the Madix group at Stanford University has studied the reactivity of oxygen on Cu(110) with CO[89] and ammonia.[90] In both cases they have also found that the terminal oxygen atoms of the (2 × 1) islands are the most reactive, but ammonia seems to be less discriminate in its reactivity, being able to attack all types of oxygen on the surface.

An important development in catalysis lately has been the recognition of the catalytic significance of Au, previously

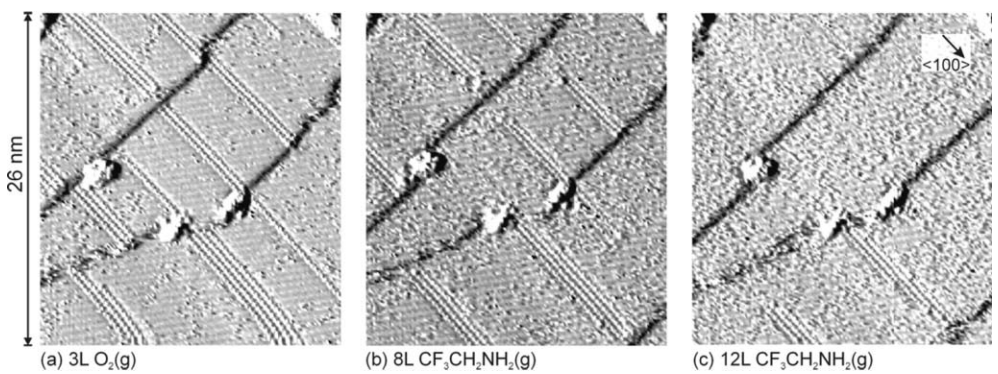

Fig. 25 STM images recorded during the reaction of 111-trifluoroethylamine with chemisorbed oxygen at a Cu(110) surface at 293 K. By fluorinating the ethylamine the basicity of the molecule has been reduced and hence the reaction rate, thus allowing the reaction to be followed more easily by STM. (a) A partial (2 × 1) oxygen adlayer. (b) & (c) images recorded during exposure to 111-trifluoroethylamine at a pressure of 1×10^{-8} mbar, showing islands shrinking in the [001] direction.[83]

thought to be an inactive material. In particular, Haruta has developed very active catalysts of Au nanoparticles supported on oxides, especially for the oxidation of CO at room temperature,[72,73] something which is very useful for pollution control. Since these discoveries, there has been controversy about the nature of the reaction, because Haruta showed that particles of very small size ($\sim$3 nm) are by far the most active for the reaction, but why is this so? Various models have been proposed relating the activity to active sites at the periphery of the particles, or to charging of the Au nanoparticles, or to hydroxylation at the edge of the catalyst. Goodman *et al.* investigated this system using model catalysts of $Au/TiO_2(110)$ to try to understand the system in greater detail.[74,75] By making particles of different sizes (Fig. 26), they were able to relate the high activity of particles of a particular size with changes in electronic structure measured on the particles with scanning tunnelling spectroscopy. It was proposed that the reactive sites are at the surface of particles which are TWO layers thick, which seem to be at the metal–non metal transition, where a real band-gap begins to open up, and is seen in the STS. The activity corresponding with different particle sizes were then measured in a high pressure cell attached to the vacuum chamber and showed a similar relationship to that of Haruta on powdered materials (Fig. 26), the implication being that when Au crystallites are prepared with an average diameter of $\sim$3 nm, then a significant fraction of them consist of the most active, two layer particles, which have quite different electronic structure, and therefore reactivity, compared with larger particles, which have a band structure closer to that of bulk gold.

Particularly beautiful images of a MoS_2 surface, fabricated *in-situ* in a vacuum system were obtained by Besenbacher and his colleagues,[59–61] as shown above in Fig. 14. The truncated triangular structures were formed by evaporation of Co and Mo onto the Au(111) surface in the presence of a low pressure of H_2S. These could be imaged in vacuum, but Besenbacher went on to try to gain insight into an essential step in the hydrodesulfurisation process, by treating these surfaces in atomic hydrogen.[59] As shown in Fig. 27, such hydrogen treatment resulted in the production of vacancies at the edge of the MoS_2 crystallites, where it was thought that S atoms had been removed. Such vacancies are obviously essential for the removal of S from organo-sulfur compounds present in hydrocarbon feedstocks. These vacancies then acted as the active sites for the subsequent adsorption of thiophene, which resulted in refilling of the vacancy.[61]

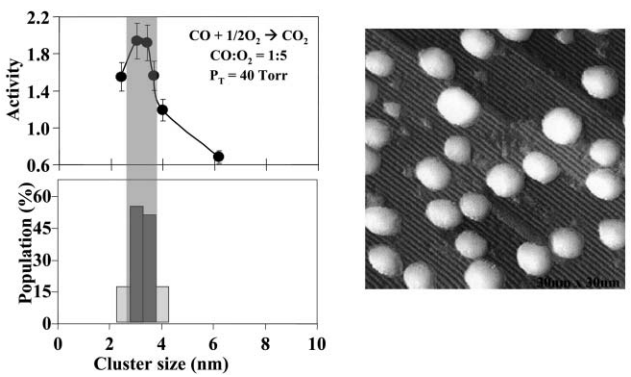

Fig. 26 Showing an STM image of a layer of gold nanoparticles fabricated onto $TiO_2(110)$ (right panel). The left panel shows the activity dependence on average particle size for such layers (top panel), compared with the fraction of two layer thick particles.[74,75]

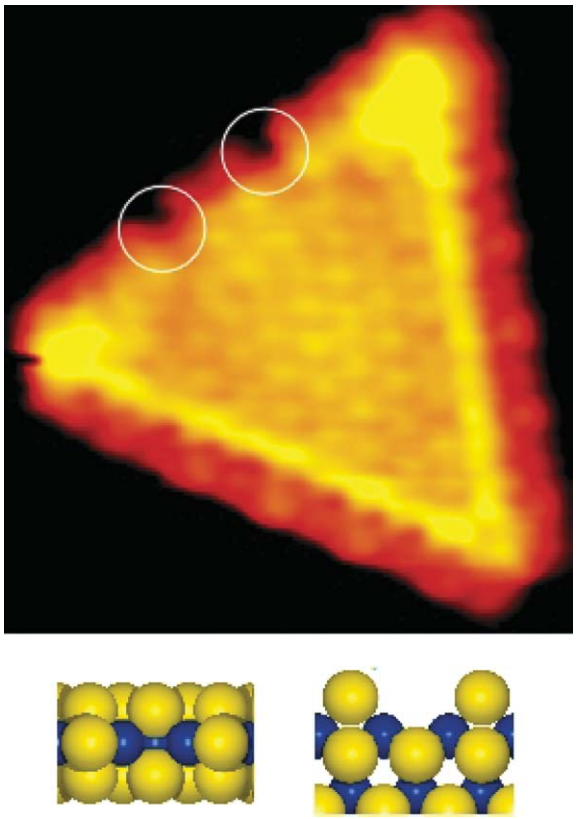

Fig. 27 An image of a MoS_2 catalyst crystallite, showing the formation of S vacancies after reduction by atomic hydrogen, and ball model structures in the lower panel. These sites are proposed by Besenbacher *et al.* to be the active sites for desulfurisation reactions.[59] ©American Physical Society 2000.

7.2. STM at high pressure

Some of the first results were presented by Somorjai and his colleagues in 1993[91,92] and these are summarised in a review article in 1996.[93] Here it was shown that the surface of Pt(110) was very dynamic under high pressures of simple gases, H_2, CO, O_2. In about one atmosphere of the gas the surface showed gross changes in terms of large scale faceting, varying its detailed morphology with the different gases used. This study immediately showed the difficulties of such work, that is, the dynamics and roughening of the surface makes atomic resolution imaging difficult. However, at lower pressure a carefully prepared CO structure could be resolved at molecular resolution. The particularly interesting point about this was that the structure under high pressure conditions was significantly different from that found in vacuum conditions. On Pt(111), for instance, CO presents a structure that repeats approximately every 5th substrate atom, giving a '(5 $\times$ 5)' relation to the underlying Pt(111). This is not entirely surprising, since it had been well known that the heat of

adsorption of CO is strongly coverage dependent, due to large repulsive interactions between CO molecules at high packing, that is, at close approach of CO molecules to one another. At higher pressures more molecules can be packed in to the adlayer *at equilibrium*, due to the higher adsorption rate, and the coverage is higher than for structures imaged before at low pressures. It is, however, more surprising that molecular resolution could be obtained at all since the system is in dynamic equilibrium, with significant rates of both adsorption and desorption.[94]

Somorjai has also proposed the idea of the "Flexible Surface"[95] as being a prerequisite for high activity in catalysis, partly as a result of STM imaging of reacting systems at high pressure. By way of example of this work, Fig. 28 shows a Pt(111) surface involved in the hydrogenation of cyclohexene,[96] in which the reactivity can be measured at the same time as the imaging. In cyclohexene alone an ordered surface structure of adsorbate is seen, but no reactivity can be measured, but when hydrogen is included hydrogenation takes place at a measurable rate, but no stable structures can be imaged. When CO is introduced into this mixture, then the reaction is poisoned by the CO, and once again ordered structures may be observed. Somorjai concludes that the surface needs to be dynamic for reactivity to occur, that is, it must be mobile, flexible, to enable sites to open up on the surface for gas phase molecules to adsorb and for reaction to take place. Similar behaviour is seen for other molecules and surfaces.[97]

An important drawback with high pressure work on low area samples such as single crystals is purity of the reacting gases. Since turnover numbers are usually very much lower than collision rates with the surface (turnover frequencies at 1 bar pressure is $\sim 1\ s^{-1}$, whereas collision rates are $\sim 10^9\ s^{-1}$), then a strongly adsorbing and unreactive molecule can block the surface and dominate the surface structure. When CO is used as a reactive gas, volatile metal-carbonyls can be produced which can contaminate the surface. These are problems in all high pressure surface science which must be overcome. These problems have been highlighted by Laegsgaard *et al.* for STM studies, in trying to study the adsorption of hydrogen on Cu(110) at high pressure.[98] Essential to such work is i) the use of ultra-pure gases ii) in-line purification of the gases used iii) use of unreactive materials in gas lines and reaction cells (*e.g.* use of quartz, and gold coatings) iv) the use of small volume reaction systems.

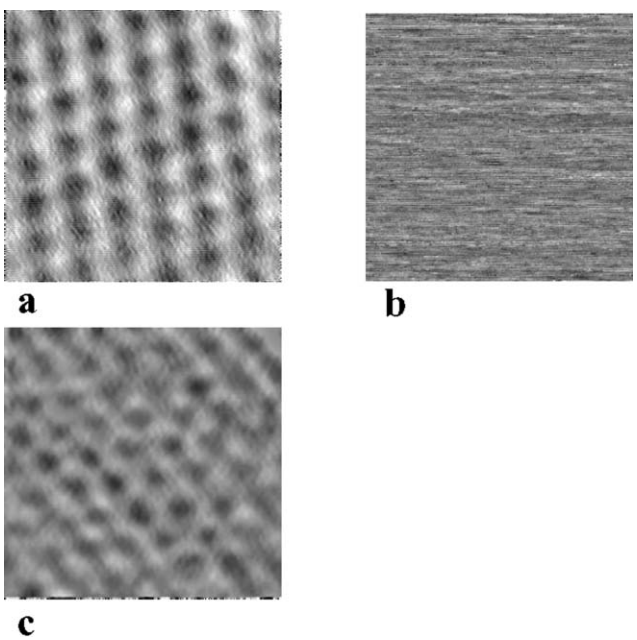

Fig. 28 (a) 37 Å × 37 Å STM image of Pt(111) exposed to 2×10^{-5} Torr cyclohexene, at which point the surface is catalytically inactive; (b) 50 Å × 50 Å image of Pt(111) exposed to 200 mTorr hydrogen, 20 mTorr cyclohexene, in this condition the catalyst is producing both cyclohexane and cyclohexene; (c) 90 Å × 90 Å image of Pt(111) in the presence of 200 mTorr hydrogen, 20 mTorr cyclohexene and 5mTorr CO, the catalytic activity has ceased.

7.3. STM at high temperature

The difficulty of trying to image surfaces at high temperature is a simple one, that is, when the sample is held at a high temperature with respect to the rest of the instrument (typically a large vacuum system) then there are significant temperature gradients which can lead to large and often anisotropic expansion of the sample under investigation. Further, since elements of the microscope are not stable at elevated temperatures (*e.g.* the piezoelectric devices depole at ~150 °C), then the whole instrument cannot be operated isothermally at high temperature. Since, for atomic resolution, we require lateral resolution of, at minimum, ~1 Å, then the movement rate of the surface beneath the tip needs to be less than about 10 Å min^{-1}, which is extremely difficult for normal designs of sample holder, which usually have a good thermal connection to the rest of the instrument. The solutions to this problem have been described by Frenken *et al.*,[99–101] and essentially involve good design of the sample holder to minimise the thermal connection of the high temperature sample to the rest of the instrument and placement of the scanning tip close to the centre of expansion of the sample holder. The resulting sample holder is usually of moderately complex design and has, additionally, to be moveable within the vacuum chamber to allow for sample cleaning and dosing.

One of the first commercial developments of this type of design was applied to the study of surface reactions at high temperature as described by Bowker *et al.*[102,103] By way of example, Fig. 29 shows the reaction of formic acid with a Cu(110) surface at 353 K.[103] Here it can be seen that the reactivity is very complicated indeed and involves several stages of changes of adsorbate and surface morphology. First of all, formic acid reacts very efficiently with high sticking probability and removes oxygen to the gas phase as water. However, as seen in Fig. 29, this occurs by the growth of p(4 × 1) strings of formate on the surface. This structure is a bulky one, taking up a large amount of surface per formate adsorbed and results in compression of the remaining oxygen into the relatively unreactive c(6 × 2) structure. The surface then ends as a mixed layer of c(6 × 2)-O and p(4 × 1) formate.

Onishi and Iwasawa were also early in applying high temperature STM to surface reactions. They used it to observe the oxidation of TiO_2(110) *in situ*;[104] the oxygen reacts by

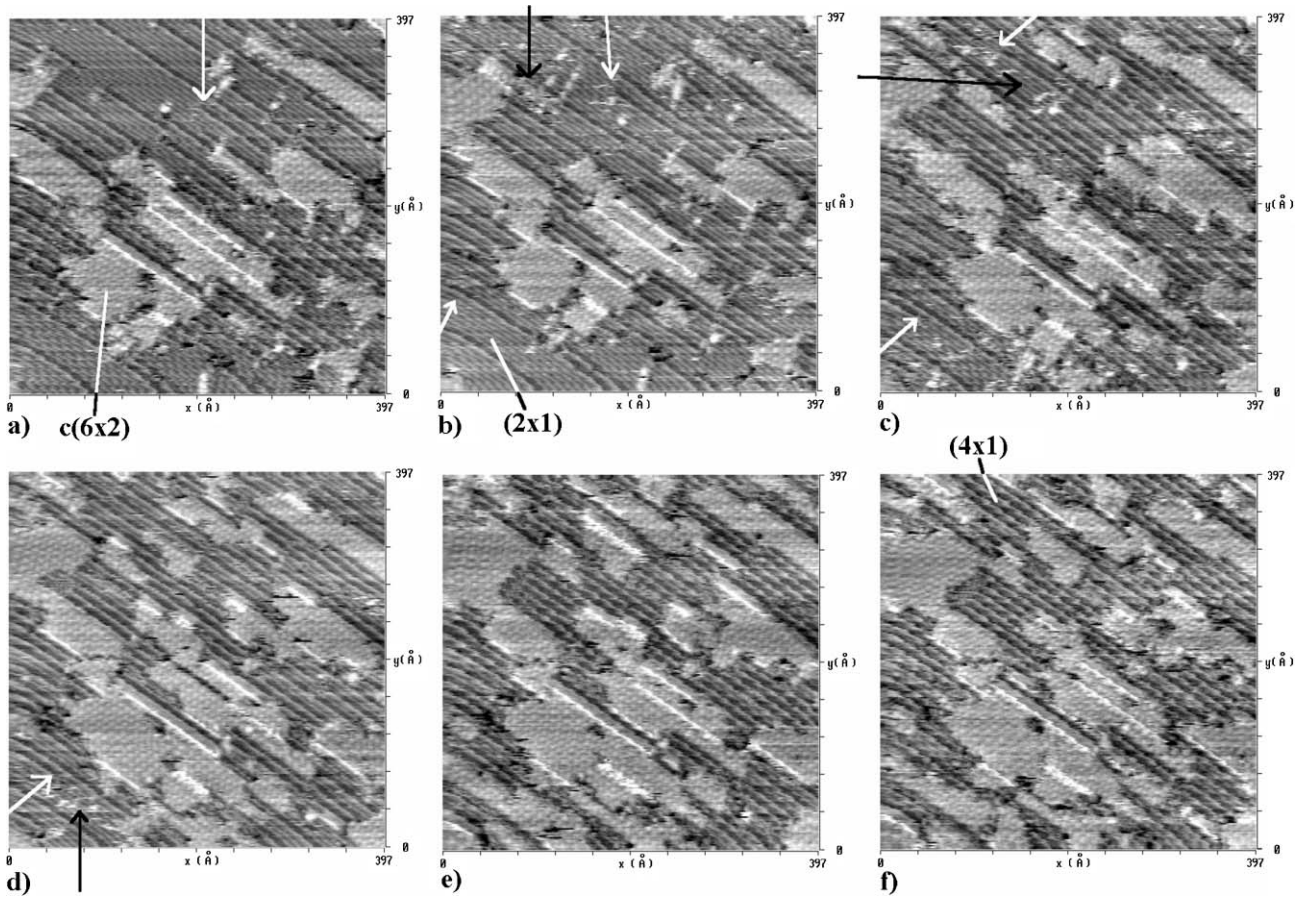

Fig. 29 Formic acid reaction with (2 × 1)-oxygen on Cu(110) at 353 K. During this sequence oxygen is removed to the gas phase as water, and formate is adsorbed onto the surface. It initially forms strings in the [001]-direction, which grow with time (arrows), and build up to form a (4 × 1) structure. At the same time remaining areas of (2 × 1) oxygen are compressed up into patches of the higher coverage c(6 × 2) structure.[103] All images 39.7 × 39.7 nm.

growing new layers of titania at the surface, seen by the island growth on the surface (Fig. 30). Such reactivity has been confirmed in more detail by Bowker *et al.*,[105,106] and this work shows direct evidence that titania growth occurs by the diffusion of interstitial Ti^{3+} to the surface where it is oxidised.

7.4. STM under catalytically realistic conditions

A number of workers are attempting to image model catalyst surfaces under realistic conditions of both high temperature and pressure. Frenken, for instance, has presented an elegant design of tiny STM for use in a flow reactor.[100,107] Here the STM tip alone is inside the reactor, and is separated from the rest of the instrument by a very small flexible ring through which the tip passes (Fig. 31). This still allows x,y,z motion of the tip while forming a tight seal. The reactor is less than 1 cm^3 and the system can operate at up to 5 bar and at temperatures between 300–425 K, with flows of up to 10 ml min^{-1}. They have examined the CO oxidation reaction on Pt(110)[107] and some of the STM results are shown in Fig. 32. This is a system which shows several different structures; the clean surface is a (1 × 2) missing row reconstruction, while the adsorption of CO usually lifts this reconstruction to produce the normal termination (1 × 1). This reaction is known to exhibit high and low rate branches, which correspond with surfaces dominated by oxygen atoms and CO molecules respectively. In a reaction mix in which the CO ratio is high the surface looks smooth and the reaction rate is low, and the surface is dominated by adsorbed CO, a layer on which oxygen dissociation is very difficult. However, upon increasing the oxygen ratio the reaction rate increases significantly and, at the same time the surface becomes much rougher, and is associated with an oxidic surface. Upon increasing the CO pressure again the surface becomes smooth, similar to the initial surface, and the reaction rate is again low. Thus the bistability of the reaction is reflected in changes in gross morphology of the surface.

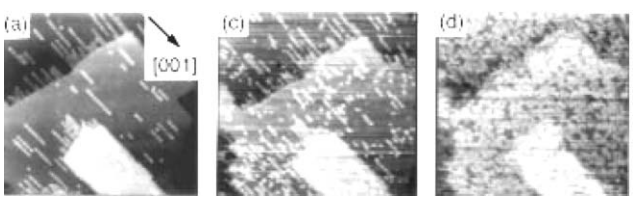

Fig. 30 STM images showing the growth of new TiO_2 layers on TiO_2(110) at 800 K, in the presence of a low pressure of oxygen;[104] the new layer is seen as strings of titania growing on the original surface. ©American Physical Society 1996.

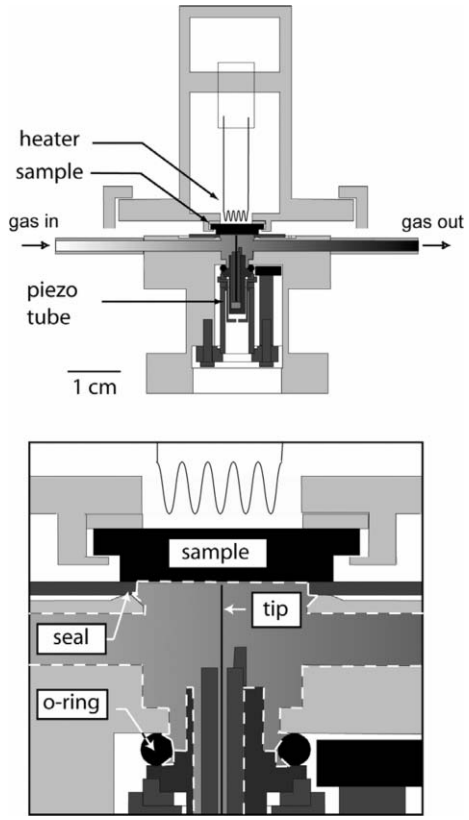

Fig. 31 Schematic cross section of the 'Reactor-STM' designed by Frenken *et al.*[100] The instrument can image a surface under gas flow conditions at pressures up to 5 bar and temperatures up to 500 K. Apart from the surface of the sample, only the tip of the STM is in contact with the flowing, hot, high-pressure gas mixture. The blow-up shows how the scanning motion, generated by the external piezo element, is transferred to the STM tip inside the reactor cell *via* a flexible Viton ® o-ring. The upper side of the reactor is closed by the sample surface that is pressed against a Kalrez seal. The volume of the cell, which is indicated by the dashed white line, is only 0.5 ml. With kind permission of Springer Science and Business Media.

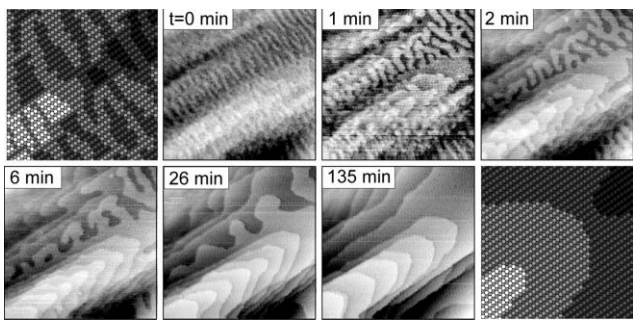

Fig. 32 Series of STM snapshots (140 nm × 140 nm) taken on Pt(110), starting immediately after introduction of 1.25 bar CO in the Reactor-STM at 425 K. The 'tiger skin' pattern in the first panel shows that the (1 × 2) to (1 × 1) transition has divided the surface into two levels, each occupying about 50% of the area, and a high density of steps. Subsequent images show the progressive reduction of the step density by coarsening of the step pattern. The elapsed time in min is indicated in each panel. The two ball models indicate the atomic-scale geometries characteristic for the starting and end situations (after ref. 100). With kind permission of Springer Science and Business Media.

7.5. STM on powdered catalysts

Besides the ability to image under realistic conditions of high temperature and pressure, it would obviously be advantageous to be able to image real catalysts at atomic resolution. Few attempts have been made to do this on realistic conditions, though there are some notable exceptions. In 1991 Besenbacher *et al.* reported a study of an industrial ammonia synthesis catalysts.[108] This is an unusual type of catalyst in that i) it is made of approximately 95% Fe metal when in use and ii) it is made by high temperature fusion, resulting in large blocks of material. As a result it was possible to make suitable, flat pieces of such a catalyst and the reduced material could be passivated by oxygen treatment to produce a thin oxide layer. This layer does not prevent tunnelling and images of the surface could be obtained, though atomic resolution was not obtained. Problems were encountered due to the presence of pores exposed at the surface of the material, but regular ridge-like features were observed. It was considered that these ridges relate to the crystallographic orientation of the surface, which is proposed (mainly from XRD work) to be predominantly (111), with multi-atomic steps of (110) orientation. However, it is clear that the structure observed is at least partly a result of the cutting procedure used to prepare a sample exposing a reasonably flat surface to enable it to be used for STM. In general it can be anticipated that studies of real, powdered catalytic materials by STM will be few, due to the fact that most are non-conductive, that they are generally very rough, and that pick-up by the tip of the powdered material is a significant problem perturbing the imaging process. Nonetheless we can anticipate successful imaging in some special cases and for particular kinds of catalysts, for instance, those consisting of metals supported on graphite.

8. Spillover in catalysis

The STM tip normally travels very close to the surface and, as a result, it might be imagined that it could interfere with surface processes. Somorjai has shown that a Pt tip can cause enhanced reactivity at a Pt surface.[109,110] A surface with hydrocarbons deposited reacted when the tip was scanned over the surface in the presence of background hydrogen to remove the carbonaceous species. This occurred by spillover of hydrogen atoms from the tip to the hydrocarbon on the surface to fully hydrogenate it and resulted in the desorption of the saturated species.[109] They could also be removed by oxidation.[110]

Fig. 33 shows an important example of this spillover phenomenon on a model nanoparticulate catalyst, which has been directly imaged *in-situ*, for the first time. In this case the model catalyst consisted of Pd nanoparticles of ~4 nm diameter, produced by MVD (metal vapour deposition) and by annealing of the layer to 673 K. When exposed to a low pressure of oxygen gas, spillover of oxygen from the Pd nanoparticles onto the surrounding TiO_2 surface occurred. The spillover region can be seen as the ring of material extending a few nanometres from the particles.[111–114] In Fig. 33 the role of spillover is to supply oxygen atoms from the Pd surface, where oxygen dissociates much more efficiently than on the oxide, onto the surrounding titania where additional

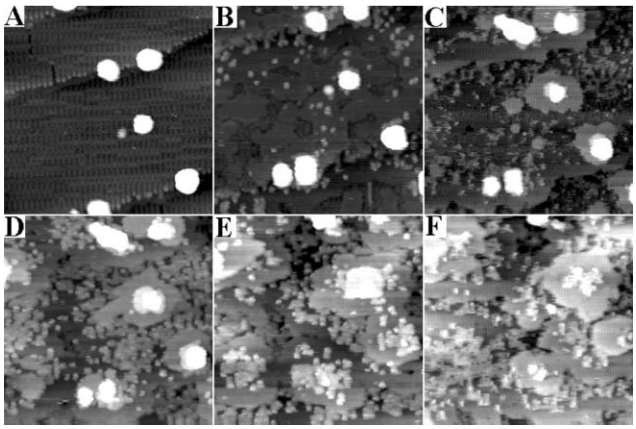

Fig. 33 A sequence of images showing the reaction of oxygen with Pd nanoparticles on TiO2(110) at 673 K.[113] A is before reaction, and B–F is a sequence after exposure to a low pressure of gas phase oxygen. The oxygen adsorbs at the Pd and spillover to the adjacent titania then occurs (seen most clearly in C). The spillover oxygen grows new titania layers close to the particle much faster than elsewhere on the surface. Image size 42 × 42 nm.

titania layers grow faster locally due to the enhanced oxygen supply. The enhancement of growth rate is a factor of 20 or so.[113]

9. The 'Strong metal–support interaction', SMSI

This effect was reported by Tauster *et al.* in 1978.[114–116] The SMSI effect occurs when some transition metals, supported on reducible oxides, are heated in a reducing atmosphere. Tauster observed that the bonding of CO to the surface of the metal was severely weakened after this treatment, and the reactivity for catalytic reactions was strongly affected, sometimes positively, often negatively.[117,118] Models were proposed which can be summarised as i) alloy formation ii) electronic metal–support interactions and iii) encapsulation. Although much evidence pointed to the latter of these there was, until, recently no atomically-resolved direct evidence for it, although TEM studies had shown evidence of the encapsulation.[119,120] Recent work by the Diebold group at Tulane,[121,122] the Bowker group at Reading and Cardiff,[123,124] and the Granozzi group at Padua[125,126] has defined this effect more clearly, at least on model catalysts. It appears that the surface becomes encapsulated in a thin layer film, which can be resolved at atomic resolution, as shown in Fig. 34. Here the catalysts studied were Pt/Ti(110) by Diebold and Pd/Ti(110) by Bowker. In both cases similar (but different) structures were found, which consisted of a zig-zag arrangement of surface atoms, which basically reveals a kind of surface alloy comprising both metal and Ti atoms in a layer with oxygen also present. Evidence from the Bowker group indicates that this layer is present as Ti^{2+} and is certainly not Ti^{4+}. Bowker has shown that these kinds of layers do indeed show the classical SMSI effect, significantly destabilising the adsorption strength of CO, as shown in Fig. 35.[127] Although much still needs to be done on this, it is clear that Ti ions are transported from the TiO_2 (which, in such work, is in a slightly reduced state) to the surface of the metal particle, thus deactivating it. Whether this

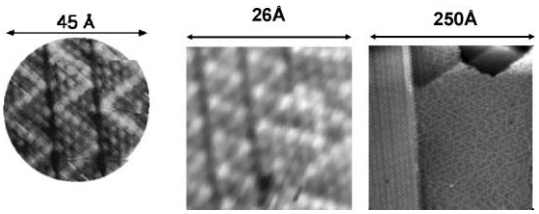

Fig. 34 Zig-zag structures formed at the surface of Pt (left),[121,122] ©American Physical Society 2000, and Pd (centre and right)[123,124] nanoparticles anchored to the TiO_2(110) surface. The structures are very similar, but differ in the number of atoms in the arms of the zig-zag (5 for Pt and 3 for Pd). The right hand image shows the co-existence of large domains of the zig-zag structure on Pd, together with domains of a 'pinwheel' arrangement;[123,124] © 2005 with permission from Elsevier. There is currently much debate about the nature of these structures—whether they are a titania layer only on the nanoparticles, or whether they are a mix of Ti and Pd or Pt is not yet certain.[121–126]

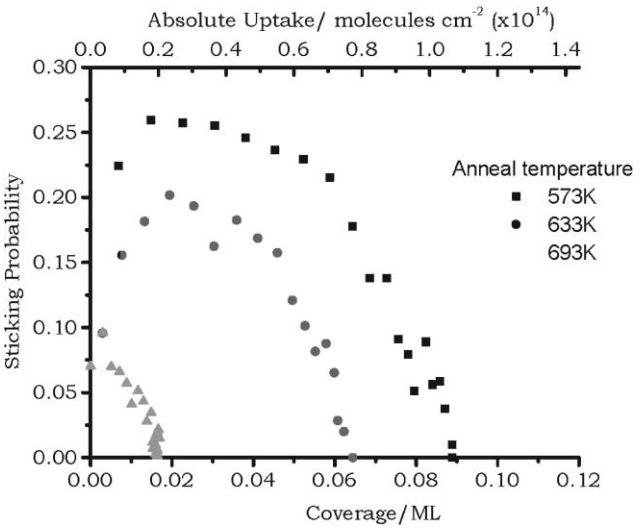

Fig. 35 Molecular beam measurements of the effect of annealing a layer of Pd nanoparticles on TiO_2(110) upon the sticking probability and uptake of CO by the sample. The adsorption is greatly diminished by heating the layer to only ~700 K, a manifestation of the SMSI effect.[127]

layer is an intermetallic-like alloy[124,128] or a complete titania layer as proposed by Diebold and Granozzi,[121,122,125,126] remains to be clarified.

10. The future

The examples above show that surface science and STM imaging has come a long way in the investigation of the nanoscale nature of catalysis at the gas–solid interface. A great deal of emphasis has been placed by the catalytic community on the importance of *in-situ* and *in-operando* studies, especially since, even within the catalytic community, few examples of this approach have been described. STM has the advantage that it can operate *in-situ* at high pressures and at elevated temperatures. This ability, combined with the potential for atomic resolution of the active site, gives STM an invaluable role in the future for understanding the nature of species and active sites during a catalytic reaction.

However, there are still hurdles to be overcome. Often catalytic turnover is very fast on the STM timescale. If we consider a catalytic turnover frequency of, say, 1 s^{-1}; this means that for an image size of 100 × 100 atoms, all of them will have reacted in one second (assuming , that is, that all sites are active). Standard scanning times might be ~30 seconds. Clearly, on such a timescale the surface will simply be an unresolved blur of activity between sequential images. The scanning time has to be significantly faster than this, probably ~0.1 second scan times will be needed for *in-situ* imaging under realistic conditions of normal turnover. In turn this requires line frequencies of ~1 ms, approximately 10 μs scan time between atoms. Even then, 10% of atoms will have transformed in the imaging time. Developments are in place regarding fast scanning,[129] though whether these will be achievable under conditions of high temperature and pressure remains to be seen. Of course, it is possible to study reactions of much lower turnover rate at more normal scan rates, but for many reactions this will require departure from the optimum activity conditions (*e.g.* by using abnormally low temperatures for the reaction).

There is no doubt that reactions are now being studied *in-situ* and there is further no doubt that this will advance in pressure, temperature and time resolution of catalysis, into the realm of relevant turnover frequency where industrial reactions are carried out.

More effort will also be devoted to more realistic versions of real catalysts, by both more sophisticated preparation of model materials that come close to resembling the relatively complex systems (*e.g.* including promoters) used in industry, and by the application to real, powdered catalysts that are anchored and prepared in an appropriate manner.

References

1 M. Knoll and E. Ruska, *Z. Physik.*, 1932, **78**, 318.
2 E. W. Muller, *Z. Physik.*, 1951, **131**, 136.
3 J. Soares and M. Bowker, *Appl. Catal., A*, 2005, **291**, 136–44.
4 G. Binnig and H. Rohrer, *Helv. Phys. Acta*, 1982, **5**, 726.
5 G. Binnig, H. Rohrer, Ch. Gerber and E. Weibel, *Phys. Rev. Lett.*, 1982, **49**, 57.
6 G. Binnig, *Nobel Prize Address*, 1986(http://nobelprize.org/nobel_prizes/physics/laureates/1986/binnig-lecture.pdf).
7 *Nobel Lectures in Physics 1981–90*, ed. G. Ekspong, World Scientific, Singapore, 1993.
8 E. Ruska, Nobel Prize Address, 1986, http://nobelprize.org/nobel_prizes/physics/laureates/1986/ruska-lecture.pdf.
9 G. Binnig, H. Rohrer, Ch. Gerber and E. Weibel, *Phys. Rev. Lett.*, 1983, **50**, 120.
10 B. Stipe, M. Resaei and W. Ho, *Phys. Rev. Lett.*, 1997, **79**, 4397.
11 R. Wiesendanger, *Scanning Probe Microscopy and Spectroscopy*, Cambridge University Press, Cambridge, 1994.
12 C. J. Chen, *Introduction to Scanning Tunneling Microscopy*, OUP, Oxford, 1993.
13 D. A. Bonnell, *Prog. Surf. Sci.*, 1998, **57**, 187.
14 J. A. Stroscio, R. M. Feenstra and A. P. Fein, *Phys. Rev. Lett.*, 1986, **57**, 2579.
15 M. Bowker, R. Bennett, R. Smith and P. Stone, *unpublished data.*.
16 J. Tersoff and D. R. Hamann, *Phys. Rev. B: Condens. Matter Mater. Phys.*, 1985, **31**, 805.
17 B. Stipe, M. Rezaei and W. Ho, *Science*, 1998, **280**, 1732.
18 M. Bowker, L. Bowker, R. Bennett, P. Stone and A. Ramirez-Cuesta, *J. Mol. Catal. A: Chem.*, 2000, **163**, 221–32.
19 M. Klimenkov, S. Nepijko, H. Kuhlenbeck, M Baumer, R. Schlogl and H.-J. Freund, *Surf. Sci.*, 1997, **391**, 27.
20 See, for instance: F. Renner, A. Stierle, H. Dosch, D.M. Kolb and J. Zegenhagen T.-L. Leeand, *Nature*, 2006, **439**, 707.
21 S. Francis, F. Leibsle, S. Haq, N. Xiang and M. Bowker, *Surf. Sci.*, 1994, **315**, 284.
22 F. Leibsle, S. Francis, S. Haq and M. Bowker, *Surf. Sci.*, 1994, **318**, 46–60.
23 M. Bowker, *Top. Catal.*, 1996, **3**, 461.
24 S. Poulston, A. Jones, R. Bennett and M. Bowker, *J. Phys.: Condens. Matter*, 1996, **8**, L1.
25 A. Jones, S. Poulston, R. Bennett and M. Bowker, *Surf. Sci.*, 1997, **380**, 31–44.
26 W. Crew and R. J. Madix, *Surf. Sci.*, 1996, **349**, 275.
27 B. Lang, R. W. Joyner and G. A. Somorjai, *Surf. Sci.*, 1972, **30**, 440.
28 R. W. Joyner and G. A. Somorjai, *Surf. Sci.*, 1972, **30**, 454.
29 K. Baron, D. Blakely and G. A. Somorjai, *Surf. Sci.*, 1974, **41**, 45.
30 S. P. Singh-Boparai, M. Bowker and D. A. King, *Surf. Sci.*, 1975, **53**, 55.
31 D. Adams and L. Germer, *Surf. Sci.*, 1971, **27**, 21.
32 G. E. Rhead, *Surf. Sci.*, 1975, **47**, 207.
33 N. D. Lang, *Phys. Rev. Lett.*, 1986, **56**, 1164.
34 L. Ruan, F. Besenbacher, I. Stensgaard and E. Laegsgaard, *Phys. Rev. Lett.*, 1993, **70**, 4079.
35 E. Vestergaard, R. Vang, J. Knudsen, T. Pedersen, T. An, E. Lægsgaard, I. Stensgaard, B. Hammer and F. Besenbacher, *Phys. Rev. Lett.*, 2005, **95**, 126101.
36 Y. Gauthier, R. Baudoing-Savois, J. Bugnard, W. Hebenstreit, M. Scmid and P. Varga, *Surf. Sci.*, 2000, **466**, 155.
37 J. Jacobsen, L. Nielsen, F. Besenbacher, I. Stensgaard, E. Laegsgaard, T. Rasmussen, K. Jacobsen and J. K. Norskov, *Phys. Rev. Lett.*, 1995, **75**, 489.
38 H. Kuhlenbeck and H.-J. Freund,'Structure and Electronic Properties of Ultra Thin Oxide Films on Metallic Substrates', in *The Chemical Physics of Solid Surfaces and Heterogeneous Catalysts*, ed. D. A. King and D. P. Woodruff, Elsevier, Amsterdam, 1997, p. 340.
39 H.-J. Freund, M. Baumer and H. Kuhlenbeck, *Adv. Catal.*, 2000, **45**, 333.
40 J. Libuda and H.-J. Freund, *Surf. Sci. Rep.*, 2005, **57**, 157.
41 W. McLean, C. Colmenares, R. Smith and G. A. Somorjai, *J. Phys. Chem.*, 1983, **87**, 788.
42 M. Levin, M. Salmeron, A. T. Bell and G. A. Somorjai, *J. Chem. Soc., Faraday Trans. 1*, 1987, **83**, 2061.
43 C. T. Campbell, K. Daube and J. M. White, *Surf. Sci.*, 1987, **182**, 458.
44 S. Fu and G. A. Somorjai, *Surf. Sci.*, 1990, **237**, 87.
45 Ph. Avouris and R. Wolkow, *Appl. Phys. Lett.*, 1989, **55**, 1074.
46 A. Boffa, H. Galloway, P. Jacobs, J. Benitez, J. Batteas, M. Salmeron, A. Bell and G. A. Somorjai, *Surf. Sci.*, 1995, **326**, 80.
47 J. Schoiswohl, S. Surnev and F. P. Netzer, *Top. Catal.*, 2005, **36**, 91.
48 M. Bowker, P. Stone, R. Smith, E. Fourre, M. Ishii and N. H. de Leeuw, *Surf. Sci.*, 2006, **600**, 1973–81.
49 P. Stone, M. Ishii and M. Bowker, *Surf. Sci.*, 2003, **537**, 179–90.
50 M. Klimenkov, S. Nepijko, H. Kuhlenbeck and H.-J. Freund, *Surf. Sci.*, 1997, **385**, 66.
51 P. W. Tasker, *J. Phys. C: Solid State Phys.*, 1979, **12**, 4977.
52 M. Kulawik, N. Nilius, H.-P. Rust and H.-J. Freund, *Phys. Rev. Lett.*, 2003, **91**, 256101.
53 G. Ceballos, Z. Song, J. Pascual, H.-P. Rust, H. Conrad, M. Bauer and H.-J. Freund, *Chem. Phys. Lett.*, 2002, **359**, 41.
54 G. Kresse, M. Schmid, E. Napetschnig, M. Shishkin, L. Kohler and P. Varga, *Science*, 2005, **308**, 1440.
55 S. Degen, A. Krupski, M. Kralj, A. Langner, C. Becker, M. Sokolowski and K. Wandelt, *Surf. Sci.*, 2005, **576**, L57.
56 S. Degen, C. Becker and K. Wandelt, *Faraday Discuss.*, 2004, **125**, 343.
57 B. K. Min, W. T. Wallace, A. K. Santra and D. W. Goodman, *J. Phys. Chem. B*, 2004, **108**, 16340.
58 S. Wendt, Y. D. Kim and D. W. Goodman, *Prog. Surf. Sci.*, 2003, **74**, 141.
59 S. Helveg, J. Lauritzen, E. Laegsgaard, I. Stensgaard, J. K. Norskov, B. S. Clausen, H. Topsoe and F. Besenbacher, *Phys. Rev. Lett.*, 2000, **84**, 951.

60 J. V. Lauritsen, S. Helveg, E. Lægsgaard, I. Stensgaard, B. S. Clausen, H. Topsøe and F. Besenbacher, *J. Catal.*, 2001, **197**, 1.
61 J. V. Lauritsen, M. Nyberg, R. Vang, M. Bollinger, B. S. Clausen, H. Topsøe, K. Jacobsen, E. Lægsgaard, J. Norskov and F. Besenbacher, *Nanotechnology*, 2003, **14**, 385.
62 H.-J. Freund, *Surf. Sci.*, 2002, **500**, 271.
63 A. Santra and D. W. Goodman, *J. Phys.: Condens. Matter*, 2002, **14**, R31.
64 N. Nilius, N. Ernst and H.-J. Freund, *Phys. Rev. Lett.*, 2000, **84**, 3994.
65 H.-J. Freund, *Catal. Today*, 2005, **100**, 3.
66 H.-J. Freund, M. Baumer, J. Libuda, T. Risse, G. Rupprechter and S. Shaikhutdinov, *J. Catal.*, 2003, **216**, 223.
67 P. Stone, S. Poulston, R. Bennett and M. Bowker, *Chem. Commun.*, 1998, 1369–70.
68 R. Bennett, P. Stone and M. Bowker, *Catal. Lett.*, 1999, **59**, 99.
69 R. Bennett, P. Stone and M. Bowker, *Faraday Discuss.*, 1999, **114**, 267–78.
70 P. Stone, R. Smith and M. Bowker, *Faraday Discuss.*, 2004, **125**, 379–90.
71 U. Diebold, *Surf. Sci. Rep.*, 2003, **48**, 74ff.
72 M. Haruta, A. Ueda, S. Tsubota and R. Torres Sanchez, *Catal. Today*, 1996, **29**, 443.
73 See, for instance,M. Haruta, *Catal. Today*, 1997, **36**, 153 and references therein.
74 M. Valden, X. Lai and D. W. Goodman, *Science*, 1998, **281**, 1647.
75 M. Valden, S. Pak, X. Liu and D. W. Goodman, *Catal. Lett.*, 1998, **56**, 7.
76 K. Wong, S. Johansson and B. Kasemo, *Faraday Discuss.*, 1996, **105**, 237.
77 B. Kasemo, S. Johansson, H. Persson, P. Thormahlen and V. P. Zhdanov, *Top. Catal.*, 2000, **13**, 43.
78 K. Hwang, M. Yang, Ji Zhu, J. Grunes and G. A. Somorjai, *J. Mol. Catal. A: Chem.*, 2003, **204–5**, 499.
79 A. Epler, Ji Zhu, E. Anderson and G. A. Somorjai, *Top. Catal.*, 2000, **13**, 33.
80 J. Zhu and G. A. Somorjai, *Nano Lett.*, 2001, **1**, 8.
81 G. Hamm, C. Becker and C. R. Henry, *Nanotechnology*, 2006, **17**, 1943.
82 J. Wilson and C. de Groot, *J. Phys. Chem.*, 1995, **99**, 7860.
83 F. Besenbacher, F. Jensen, E. Laegsgaard, K. Mortensen and I. Stensgaard, *J. Vac. Sci. Technol., B*, 1991, **9**, 874.
84 D. Coulman, J. Wintterlin, R. J. Behm and G. Ertl, *Phys. Rev. Lett.*, 1990, **64**, 1761.
85 F. Besenbacher and J. Norskov, in *The Chemical Physics of Solid Surfaces and Heterogeneous Catalysis*, ed. D. A. King and D. P. Woodruff, Elsevier, 1993, ch. 15.
86 P. R. Davies, D. Edwards and M. Parsons, *Surf. Sci.*, submitted.
87 P. R. Davies, D. Edwards and D. Richards, *J. Phys. Chem. B*, 2004, **108**, 18630.
88 A. F. Carley, P. R. Davies, D. Edwards, R. Jones and M. Parsons, *Top. Catal.*, 2005, **36**, 21.
89 W. Crew and R. J. Madix, *Surf. Sci.*, 1996, **349**, 275.
90 X.-C. Guo and R. J. Madix, *Surf. Sci.*, 1997, **387**, 1.
91 B. J. McIntyre, M. Salmeron and G. A. Somorjai, *Rev. Sci. Instrum.*, 1993, **64**, 687.
92 B. J. McIntyre, M. Salmeron and G. A. Somorjai, *J. Vac. Sci. Technol., A*, 1993, **11**, 1964.
93 G. A. Somorjai, *Z. Phys. Chem., Bd.*, 1996, **197**, 1.
94 J. Jensen, K. Rider, M. Salmeron and G. A. Somorjai, *Phys. Rev. Lett.*, 1998, **80**, 1228.
95 G. A. Somorjai, *J. Mol. Catal. A: Chem.*, 1996, **107**, 39.
96 D. Tang, K. Hwang, M. Salmeron and G. A. Somorjai, *J. Phys. Chem. B*, 2004, **108**, 13300.
97 G. A. Somorjai and G. Rupprechter, *J. Chem. Educ.*, 1998, **75**, 162.
98 E. Laegsgaard, L. Osterlund, P. Thostrup, P. Rasmussen, I. Stensgaard and F. Besenbacher, *Rev. Sci. Instrum.*, 2001, **72**, 3537.
99 P. Rasmussen, B. Hendriksen, H. Zeijklemaker, H. Ficke and J. W. Frenken, *Rev. Sci. Instrum.*, 1998, **69**, 3879.
100 B. L. M. Hendriksen, S. Bobaru and J. W. M. Frenken, *Top. Catal.*, 2005, **36**, 43.
101 B. L. M. Hendriksen, PhD thesis, Leiden University , 2003.
102 R. Bennett, S. Poulston and M. Bowker, *J. Chem. Phys.*, 1998, **108**, 6916.
103 R. Bennett, S. Poulston, I. Jones and M. Bowker, *Surf. Sci.*, 1998, **401**, 72.
104 H. Onishi and Y. Iwasawa, *Phys. Rev. Lett.*, 1996, **76**, 791.
105 R. Bennett, P. Stone, N. Price and M. Bowker, *Phys. Rev. Lett.*, 1999, **82**, 3831.
106 P. Stone, R. Bennett and M. Bowker, *New J. Phys.*, 1999, **1**, 8 (http://www.njp.org).
107 B. L. M. Hendriksen, S. Bobaru and J. W. M. Frenken, *Catal. Today*, 2005, **105**, 234.
108 F. Besenbacher, E. Laegsgaard, I. Stensgaard, P. Stoltze and H. Topsoe, *Cat. Lett.*, 1991, **8**, 273.
109 B. J. McIntyre, M. Salmeron and G. A. Somorjai, *Science*, 1994, **265**, 1415.
110 U. Schroder, B. J. McIntyre, M. Salmeron and G. A. Somorjai, *Surf. Sci.*, 1995, **331–3**, 337.
111 R. Bennett, P. Stone and M. Bowker, *Catal. Lett.*, 1999, **59**, 99–106.
112 A. J. Ramirez-Cuesta, R. A. Bennett, P. Stone, P. C. H. Mitchell and M. Bowker, *J. Mol. Catal. A: Chem.*, 2001, **167**, 171–9.
113 M. Bowker, R. A. Bennett, A. Dickinson, D. James, R. D. Smith and P. Stone, *Stud. Surf. Sci. Catal.*, 2001, **133**, 3–17.
114 S. Tauster, S. Fung and R. Garten, *J. Am. Chem. Soc.*, 1978, **100**, 170.
115 S. Tauster and S. Fung, *J. Catal.*, 1978, **55**, 29.
116 For a review, see S. Tauster, *Acc. Chem. Res.*, 1987, **20**, 389.
117 E. Ko and R. Garten, *J. Catal.*, 1981, **68**, 223.
118 D. Resasco and G. Haller, *Stud. Surf. Sci. Catal.*, 1982, **11**, 105.
119 A. Logan, E. Braunschweig and A. Datye, *Langmuir*, 1988, **4**, 827.
120 A. Datye, D. Kalakkad and M. Yao, *J. Catal.*, 1995, **155**, 148.
121 O. Dulub, W. Hebenstreit and U. Diebold, *Phys. Rev. Lett.*, 2000, **84**, 3646.
122 D. Jennison, O. Dulub, W. Hebenstreit and U. Diebold, *Surf. Sci.*, 2001, **492**, L677.
123 R. A. Bennett, C. Pang, N. Perkins, R. D. Smith, P. Morrall, R. Kvon and M. Bowker, *J. Phys. Chem.*, 2002, **106**, 4688.
124 M. Bowker, P. Stone, P. Morrall, R. Smith, R. A. Bennett, N. Perkins, R. Kvon, C. Pang, E. Fourre and M. Hall, *J. Catal.*, 2005, **234**, 172–181.
125 F. Sedona, G. Rizzi, S. Agnoli, F. Xamena, A. Papageorgiou, D. Ostermann, M. Sambi, P. Finetti, K. Schierbaum and G. Granozzi, *J. Phys. Chem. B*, 2005, **109**, 24411.
126 F. Sedona, S. Agnoli and G. Granozzi, *J. Phys. Chem. B*, 2006, **110**, 15359.
127 M. Bowker, P. Stone, R. A. Bennett and N. Perkins, *Surf. Sci.*, 2002, **497**, 155.
128 R. Nuzzo and L. H. Dubois, *Heterometallic Compounds as Models for Materials Formed at the Metal Crystallite-Oxide Support Interface*, ACS Symp. Ser. 298, ed. R. Baker, S. Tauster and J. Dumesic, ACS, Washington DC, 1986, p. 136.
129 See, for instance,M. Rost, L. Crama, P. Schakel, E. van Tol, G. van-Velzen-Williams, C. Overgauw, H. ter Horst, H. Dekker, B. Okhuijsen, M. Seynen, A. Vijftigschild, P. Han, A. Hatan, K. Schoots, R. Schumm, W. van Loo, T. Oosterkamp and J. H. Frenken, *Rev. Sci. Instrum.*, 2005, **76**, 053710.